REVIEWS OF MODERN PHYSICS VOLUME 20, NUMBER 3 JULY, 1948

Interpretation of Cosmic-Ray Phenomena

BRUNO ROSSI

*Physics Department and Laboratory for Nuclear Science and Engineering, Massachusetts Institute of Technology, Cambridge, Massachusetts**

FOREWORD

IN the present article some of the fundamental experiments on cosmic rays are described and an attempt is made to place their results into a logically consistent picture. The article does not cover the whole field of cosmic rays. The subject of air showers, for instance, has been left out and geomagnetic effects have not been discussed quantitatively. Also the historical development of cosmic-ray research has been largely overlooked. Thus, both in the text and in the references, the author may have failed to mention historically important contributions to the various subjects considered in this article. For these omissions he offers his apologies.

The author wishes to acknowledge the help given him in the preparation of this article by Mr. M. Sands, who collected a large part of the numerical data and contributed valuable discussion and criticism. He also wishes to thank the following persons who kindly made available to him some of their unpublished results: C. D. Anderson, H. Bridge, W. B. Fretter, S. E. Golian, W. E. Hazen, R. I. Hulsizer, O. Piccioni, M. Sands, R. Sard, M. Schein, H. E. Tatel, J. Tinlot, G. E. Valley, R. W. Williams, L. C. L. Yuan.

This work was supported in part by the Office of Naval Research.

I. SOME QUANTITATIVE DATA ON COSMIC RAYS

1. Definitions

Cosmic rays, as we observe them in the atmosphere, contain electrons, photons, mesons (possibly of different kinds), protons, neutrons, and heavier nuclear fragments.

The electron and the photon components are intimately related to one another, because whenever electrons are present, photons are generated by bremsstrahlung, and whenever photons are present, electrons are generated by materialization. Thus, genetically, electrons and photons form a single component which, in what follows, will be designated as the *electronic component* of cosmic rays.

It is well known that the curve which represents the coincidence rate between two or more Geiger-Mueller counters arranged on a straight line as a function of the thickness of a lead absorber placed between them shows a rather sudden change in slope at a thickness near 10 cm, being steeper for small thicknesses and flatter for large thicknesses. This fact is due to the presence in the cosmic radiation of electrons which are easily absorbable. Independently of its interpretation, it leads to an empirical separation of cosmic-ray particles into a *hard component*, which includes all particles capable of traversing a given lead thickness, and a *soft component*, which includes all particles which are capable of traversing the counter walls but are stopped by the given lead thickness. The choice of the critical thickness is, of course, somewhat arbitrary and the subdivision of cosmic-ray particles into a hard and a soft component has a meaning only because the relative intensities of the two components depends only slightly on this choice.

Cloud-chamber observations of the passage of cosmic-ray particles through lead plates provide a method for separating electrons from particles with larger masses (mesons, protons). In fact, electrons have a much larger probability than mesons or protons of producing high energy photons in the lead. Therefore, they suffer larger energy losses and are much more likely to initiate showers. Since, in cloud-chamber pictures, it is often difficult to distinguish mesons from protons, it is convenient to have a name that applies to both kinds of particles. In what follows we will designate them as *penetrating particles* (regardless of their energy). The subdivision of cosmic-ray particles into electrons

* This paper was prepared as a contribution to the 1948 Solvay Conference.

and penetrating particles is not identical to the subdivision into soft and hard component, because, while it is true that the hard component consists practically only of penetrating particles, the soft component contains beside electrons also mesons and protons of low energy.

To facilitate a quantitative description of the various components of the cosmic radiation, we shall define the following quantities:

(a) *Directional intensity, I.* $Id\omega d\sigma dt$ represents the number of particles of a given kind incident upon the element of area $d\sigma$ during the time dt within the element of solid angle $d\omega$ perpendicular to $d\sigma$. I will be measured in cm^{-2} $sec.^{-1}$ $steradian^{-1}$. I_v will represent the value of I in the vertical direction.

(b) *Flux,* J_1. $J_1 d\sigma dt$ represents the number of particles of a given kind traversing in a downward sense a horizontal element of area $d\sigma$ during the time dt. J_1 is related to I by the equation

$$J_1 = \int I \cos\theta d\omega, \tag{1}$$

where θ is the angle between the vertical and the direction of $d\omega$ and the integration is extended over the upper hemisphere. The unit for J_1 is cm^{-2} $sec.^{-1}$.

(c) *Integrated intensity,* J_2. J_2 is defined as

$$J_2 = \int I d\omega, \tag{2}$$

where the integral is extended over all directions. J_2 is measured in cm^{-2} $sec.^{-1}$.

In this report the following notations and numerical values will be used: M = mass of the proton $= 0.935 \cdot 10^9$ ev/c^2, μ = mass of the ordinary meson $= 10^8$ ev/c^2, τ = lifetime of the ordinary meson $= 2.15 \cdot 10^{-6}$ sec., c = velocity of light $= 3 \cdot 10^{10}$ cm $sec.^{-1}$, β = value of the velocity in terms of the velocity of light, Z = atomic number, and A = atomic weight.

2. The Hard and the Soft Components at Sea Level and at Geomagnetic Latitudes Greater than 45°

To this date, no variation with geomagnetic latitude has been detected from 45° to the pole for any cosmic-ray effect (with the possible exception of the integrated intensity at very great altitudes). Therefore we shall consider together all experimental data obtained at latitudes greater than 45°.

Accurate measurements of the intensity of the hard component and of the total intensity of the corpuscular radiation (hard plus soft) were made by Greisen (G3) at 50° and at 259 m above sea level (1007-g cm^{-2} atmospheric depth). The absorber used to separate the hard from the soft component was *167 g cm^{-2} of lead.* For the hard component, after correcting for the difference between geometric length and effective length of a Geiger-Mueller counter (G4), the results were as follows:

$$I_v = 0.82 \cdot 10^{-2} \text{ cm}^{-2} \text{ sec.}^{-1} \text{ sterad}^{-1},$$
$$J_1 = 1.26 \cdot 10^{-2} \text{ cm}^{-2} \text{ sec.}^{-1},$$
$$J_2 = 1.66 \cdot 10^{-2} \text{ cm}^{-2} \text{ sec.}^{-1}.$$

In the above evaluation the decrease in the number of coincidences caused by scattering of particles out of the beam and the increase caused by showers have been neglected. The error thus introduced can be estimated by comparing the above value of J_2 with another value of the same quantity measured by Greisen (G5) with an arrangement in which scattering is practically of no consequence and the effect of showers can be corrected for. This comparison, after making allowance for the different thickness of the absorber used in the two experiments (107 g cm^{-2} instead of 167 g cm^{-2}—4 percent correction) indicates that the values of I_v, J_1, and J_2 listed above should be increased by about 4 percent to correct for the combined effect of scattering and showers. A correction of about 3 percent in the opposite direction must be applied in order to obtain the intensities at sea level (1030 g cm^{-2}). These two corrections yield the following values:

hard component:

$$I_v = 0.83 \cdot 10^{-2} \text{ cm}^{-2} \text{ sec.}^{-1} \text{ sterad}^{-1},$$
$$J_1 = 1.27 \cdot 10^{-2} \text{ cm}^{-2} \text{ sec.}^{-1},$$
$$J_2 = 1.68 \cdot 10^{-2} \text{ cm}^{-2} \text{ sec.}^{-1}. \tag{3}$$

The statistical errors of the measurements are about one percent. The systematic errors may be appreciably larger on account of the uncertainties connected with the various corrections.

As for the angular dependence, Greisen's results, in agreement with previous data, indicate

that *I varies very closely as the square of the cosine of the zenith angle.*

The total intensity is harder to measure in absolute value than the intensity of the hard component. Because of the large number of low energy particles (mainly electrons) in the cosmic radiation, the counting rate in a cosmic-ray telescope without any absorber between the counters depends critically on the wall thickness of the counters. Also the existence of any roof above the instrument is apt to influence the measurements appreciably.

In Greisen's experiments the counter walls were equivalent to a layer of 2.3 g cm^{-2} of brass between the sensitive volumes of the counters. The results of a first set of experiments (G3), after correcting for the effective length of the counters, were:

$$I_v = 1.23 \cdot 10^{-2} \text{ cm}^{-2} \text{ sec.}^{-1} \text{ sterad}^{-1},$$
$$J_1 = 1.93 \cdot 10^{-2} \text{ cm}^{-2} \text{ sec.}^{-1},$$
$$J_2 = 2.60 \cdot 10^{-2} \text{ cm}^{-2} \text{ sec.}^{-1}.$$

In a second experiment (G5) the following value of J_2 was obtained:

$$J_2 = 2.53 \cdot 10^{-2} \text{ cm}^{-2} \text{ sec.}^{-1}.$$

The difference between the two values of J_2 is hardly significant because of the statistical errors of the measurements. If real, it may be explained as due to showers the effect of which was taken into account in the second measurement but not in the first. We will, therefore, consider the second value of J_2 as the more reliable and correct the values of I and J_1 obtained in the first measurement to bring them into agreement with this value of J_2. After applying an altitude correction (which, for the total intensity, amounts to about 5 percent) we obtain the following sea level values for the total intensities and for the intensity of the soft component, as measured with 2.3 g cm^{-2} of brass between the sensitive volumes of the counters:

total intensity:

$$I_v = 1.14 \cdot 10^{-2} \text{ cm}^{-2} \text{ sec.}^{-1} \text{ sterad}^{-1},$$
$$J_1 = 1.79 \cdot 10^{-2} \text{ cm}^{-2} \text{ sec.}^{-1},$$
$$J_2 = 2.41 \cdot 10^{-2} \text{ cm}^{-2} \text{ sec.}^{-1}. \quad (4)$$

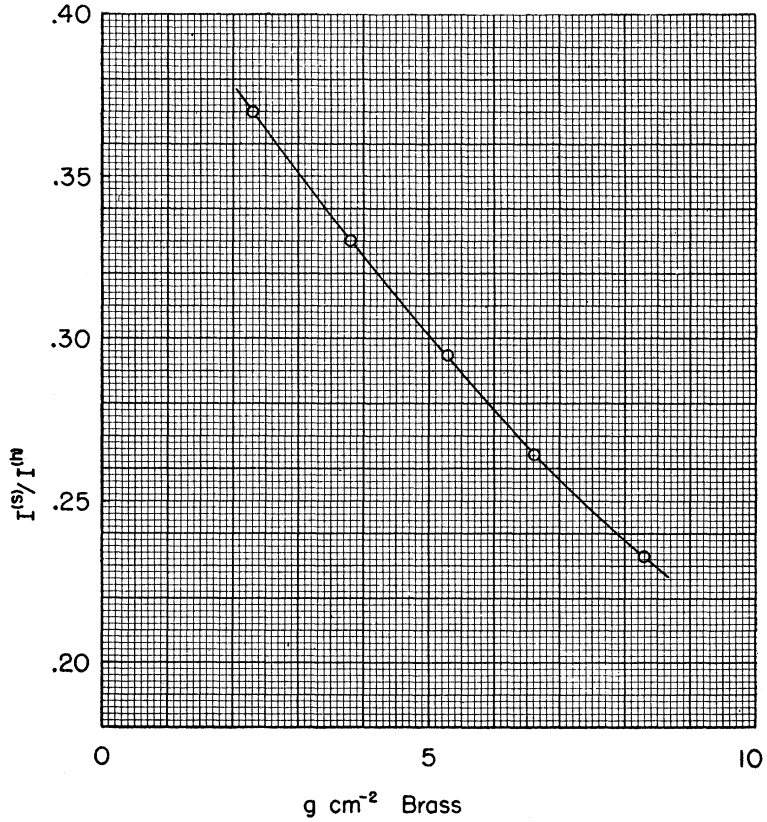

FIG. 1. Absorption curve of "soft" cosmic-ray particles in brass. The abscissa is the minimum range of the soft particles as determined by the thickness of the counter walls. The ordinate is the corresponding ratio of intensity of the soft to that of the hard component at sea level.

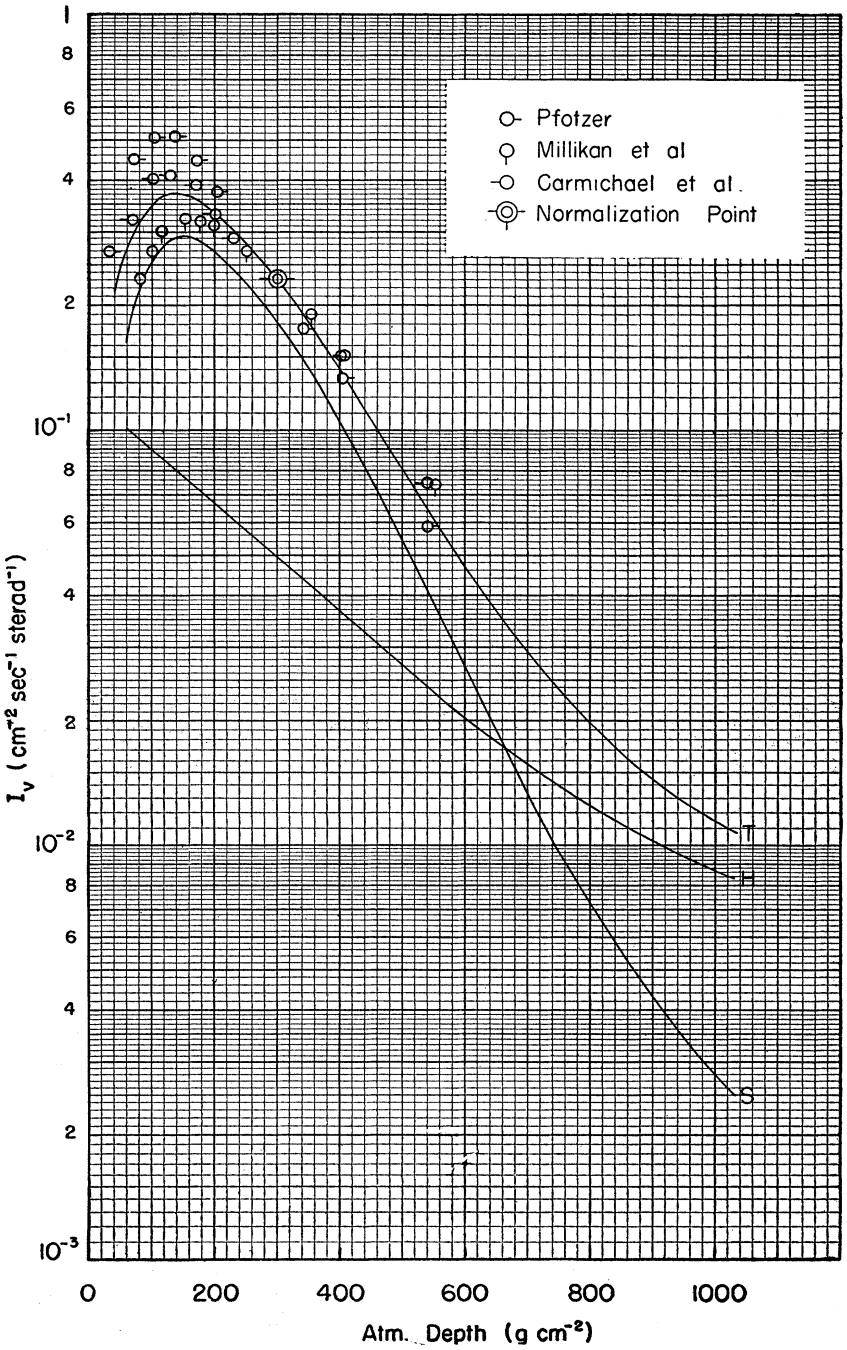

FIG. 2. The vertical intensities of the hard component (H), of the soft component (S), and of the total corpuscular radiation (T) as a function of atmospheric depth at geomagnetic latitudes greater than 45°. Minimum range of the soft particles: 5 g cm^{-2} of brass.

Soft component (by difference):

$$I_v = 0.31 \cdot 10^{-2} \text{ cm}^{-2} \text{ sec.}^{-1} \text{ sterad}^{-1},$$
$$J_1 = 0.52 \cdot 10^{-2} \text{ cm}^{-2} \text{ sec.}^{-1},$$
$$J_2 = 0.73 \cdot 10^{-2} \text{ cm}^{-2} \text{ sec.}^{-1}. \quad (5)$$

The intensities of the soft component measured with brass counters of different wall thickness can be obtained by means of the curve in Fig. 1. This curve is based upon some absorption measurements in carbon by Greisen (G5). The computation of the absorption in brass from the observed absorption in carbon was based on the

average energy losses of electrons in the two materials. This procedure is justified by the fact that most soft particles are electrons. The thickness to be considered is the *average* thickness *between* the sensitive volumes of the two extreme counters for particles distributed at random, and is approximately equal to $\pi(n-1)d/2$ where n is the number of counters and d the wall thickness of each counter.

3. Variation of the Hard and Soft Components with Altitude at Geomagnetic Latitudes Greater than 45°

Curve H in Fig. 2 represents the vertical intensity, I_v, of the hard component as a function of depth below the top of the atmosphere. The lower part of the curve (from 1030 to 616 g cm^{-2}, i.e., from sea level to 4300-m altitude) is based upon the measurements of Rossi, Hilberry, and Hoag (R4), in which the cosmic-ray telescope was well shielded against side showers. These measurements are in very good agreement with those of other authors (G3; B2). The upper part of the curve is based upon balloon and airplane measurements of Gill, Schein, and Yngve (G1). The curve is normalized at sea level to the value of I_v given in the previous section.

Curve T in Fig. 2 represents the *total* vertical intensity as a function of depth. The portion of the curve between 1030 and 250 g cm^{-2} is based upon measurements made by Sands (S2) in an airplane. In Sands' experiments the counter walls were equivalent to a 5-g cm^{-2} brass absorber between the sensitive volumes of the counters. According to Fig. 1, the vertical intensity of the soft component at sea level with counter walls of this thickness is $0.25\cdot10^{-2}$ cm^{-2} sec.$^{-1}$ sterad^{-1}. Consequently, Sands' measurements of the total intensity were normalized at sea level to a value of $(0.83+0.25)\cdot10^{-2}=1.08\cdot10^{-2}$ cm^{-2} sec.$^{-1}$ sterad^{-1}. No measurements were taken by Sands in the interval from 1030 to 616 g cm^{-2}. To fill this gap, the results obtained by Greisen at various altitudes in the mountains were used (G3). In these experiments, the wall thickness was equivalent to 2.3 g cm^{-2} of brass. It was assumed that, between 1030 and 616 g cm^{-2}, the *variation* with altitude in the intensity of the soft component is the same when measured with 2.3 as when measured with 5 g cm^{-2} of brass. For depths less than 250 g cm^{-2}, measurements of different experimenters by means of balloon-borne equipment are available (P2; M3; C1). Since in some of these measurements the ground point was not determined accurately, the balloon data were normalized to Sands' curve at the depth of 300 g cm^{-2}. As shown by the figure, the results of the various experiments differ considerably and it is not clear whether the discrepancies are due to experimental errors or to fluctuations in the cosmic-ray intensity at great altitudes. There is, therefore, great uncertainty in the value of the total intensity in the upper atmosphere. The curve drawn in Fig. 2 is some kind of an average between the various experimental data. Curve S is the difference between curves T and H and represents the vertical intensity of the soft component as a function of depth.

4. The Hard and the Soft Components Near the Equator

Curves T, H, and S in Fig. 3 represent the vertical intensities as a function of atmospheric depth near the geomagnetic equator for the total corpuscular radiation, for the hard component and for the soft component, respectively.

The sea level intensities were obtained from the values measured at latitudes greater than 45° under the assumption of a 5 percent latitude effect both for the hard and the soft component, as indicated by the recent work of Morris, Swann, and Taylor (M4).

The total vertical intensity at high altitudes was obtained from the results of Millikan, Neher, and Pickering (M3). These results were normalized by multiplying all the intensity figures given by Millikan, Neher, and Pickering by an appropriate factor chosen so as to bring the value of the intensity measured at latitudes greater than 45° and at a depth of 300 g cm^{-2} in agreement with the value given by curve T in Fig. 2.

The vertical intensity of the hard component at high altitudes was obtained from the results of Gill *et al.* (G1), again normalized to the accepted value for the intensity of the hard component at 300 g cm^{-2} and at latitudes greater than 45°. The latitude effect for the hard component

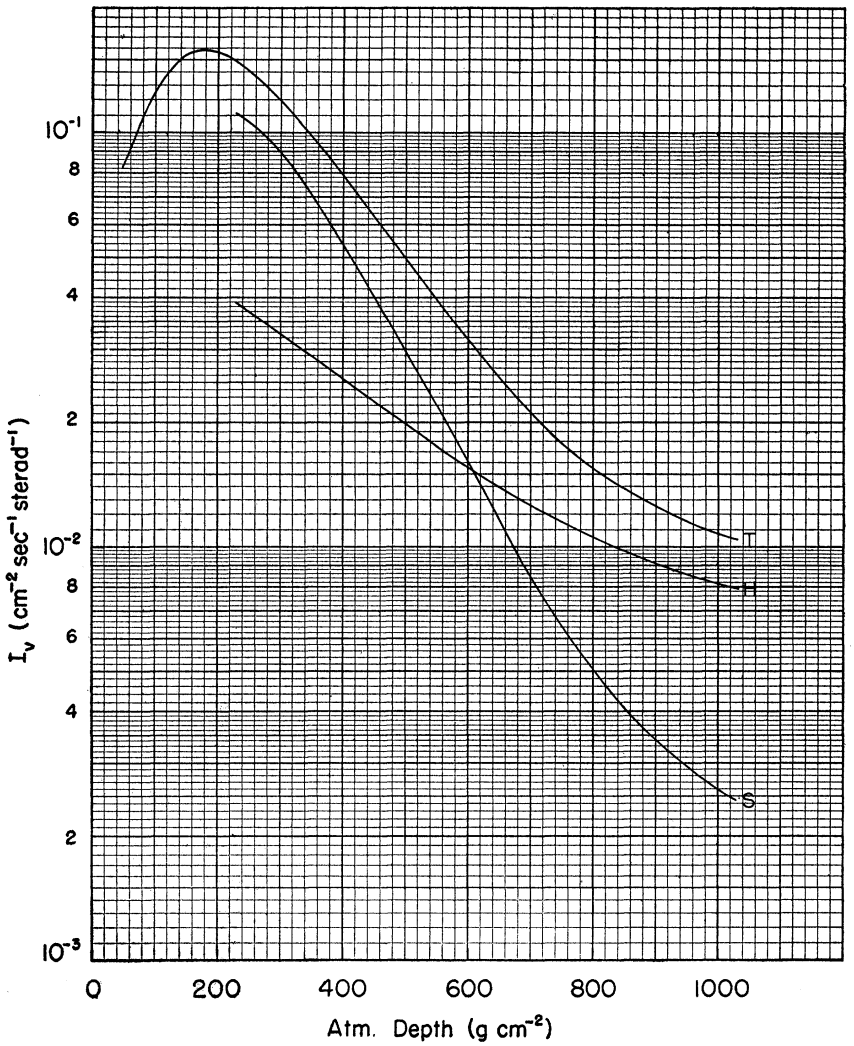

FIG. 3. The vertical intensities of the hard component (H), of the soft component (S), and of the total corpuscular radiation as a function of atmospheric depth near the geomagnetic equator. Minimum range of the soft particles: 5 g cm^{-2} of brass.

at high elevation shown by the measurements of Gill *et al.* is in good agreement with the observations of Morris *et al.* (M4). Curve S was obtained by difference from curves T and H.

5. The Momentum Spectrum of Mesons at Sea Level

As already pointed out, it is easy to distinguish electrons from penetrating particles by the cloud-chamber method. Curvature measurements of electron tracks in magnetic fields and observations of shower production in lead plates have shown that the energy spectrum of electrons at sea level falls off very rapidly with energy. From the rate of occurrence of large showers under a few centimeters of lead one concludes that, at sea level, electrons of energy greater than 10 Bev are fewer than 1 every 10,000 cosmic-ray particles (see, for instance, B7).

Penetrating particles with momenta less than about $7 \cdot 10^8$ ev/c can be separated into mesons and protons by evaluating the specific ionization from the density of their cloud-chamber tracks. This method fails for penetrating particles with momenta larger than about $7 \cdot 10^8$ ev/c. However, as will be shown later, there is evidence that, at sea level, high energy protons are very scarce (it is estimated that less than 1 percent of the penetrating particles with momenta larger than $7 \cdot 10^8$ ev/c are protons, see Section 20). There-

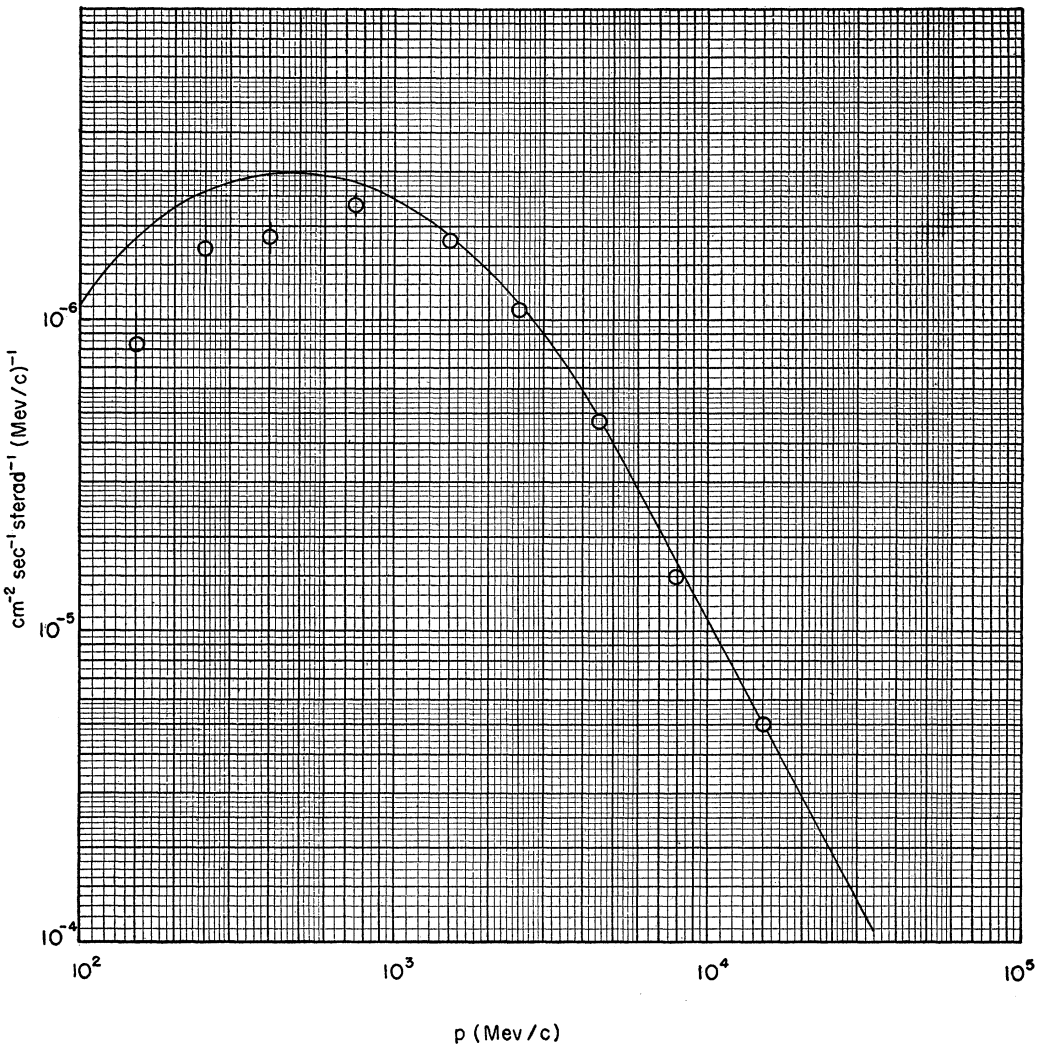

FIG. 4. Differential momentum spectrum of mesons at sea level. The circles represent experimental determinations by Wilson (W7). (*Note:* In the ordinate scale 10^{-4} and 10^{-5} should read 10^{-8} and 10^{-7}, respectively.)

fore, for the determination of the momentum spectrum of mesons at sea level from cloud-chamber pictures of cosmic-ray particles in magnetic fields, one is justified in considering as mesons all penetrating particles which cannot be shown to be different from mesons by their specific ionization.

The circles in Fig. 4 represent the differential momentum spectrum of mesons at sea level as measured by J. G. Wilson (W7), whose results are in good agreement with the previous determinations of Blackett (B6) and of other authors (J6; H5) but extend to lower momenta. The data are normalized so as to give the vertical intensity of mesons per 10^6 ev/c momentum range. Since it appears that the relative number of particles with momenta larger than 2 Bev is a quantity which can be particularly well determined from the cloud-chamber measurements, the normalization factor was chosen so as to bring the number of particles with momenta larger than 2 Bev/c in agreement with the absolute value for this quantity determined from absorption measurements (see Section 6). The curve in Fig. 4 shows the most reasonable estimate of the momentum spectrum which can be made at the present time

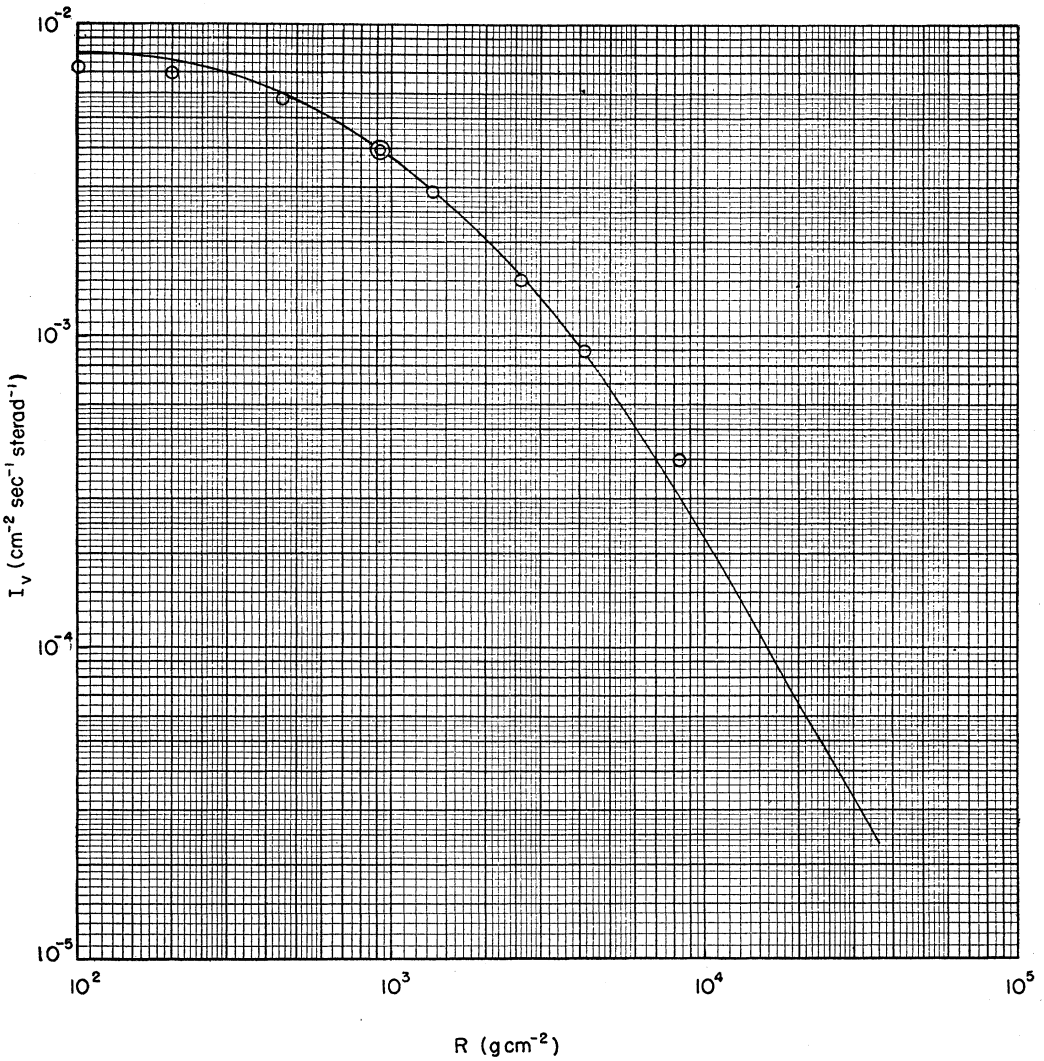

FIG. 5. Integral range spectrum of mesons at sea level. The range is measured in g cm^{-2} of air. The circles represent data obtained from the measurement of the momentum spectrum (W7), normalized at $R=920$ g cm^{-2} (double circle).

by considering both the measurements of magnetic deflection and the absorption measurements (see Section 6).

With regard to the *nature* of the mesons observed at sea level, while no direct information exists on high energy mesons, it is found that the great majority, if not all, of the mesons which arrive at sea level with a sufficiently low energy for their mass to be determined by cloud-chamber experiments, or which are brought into this low energy range by passage through matter, are "ordinary" mesons with mass about equal to 200 electron masses (B5; F1). Evidence for mesons of larger mass has been found in the examination of photographic emulsions exposed to cosmic rays at high elevation (L1; L2). The failure to find any appreciable number of such heavy mesons by the cloud-chamber method at sea level may be explained by the assumption that they decay with a very short lifetime into ordinary mesons, so that they can only be observed near the place where they are produced.

6. The Range Distribution of Mesons at Sea Level

Ehmert (E1) and Wilson (W8) have measured the vertical intensity of cosmic rays at various

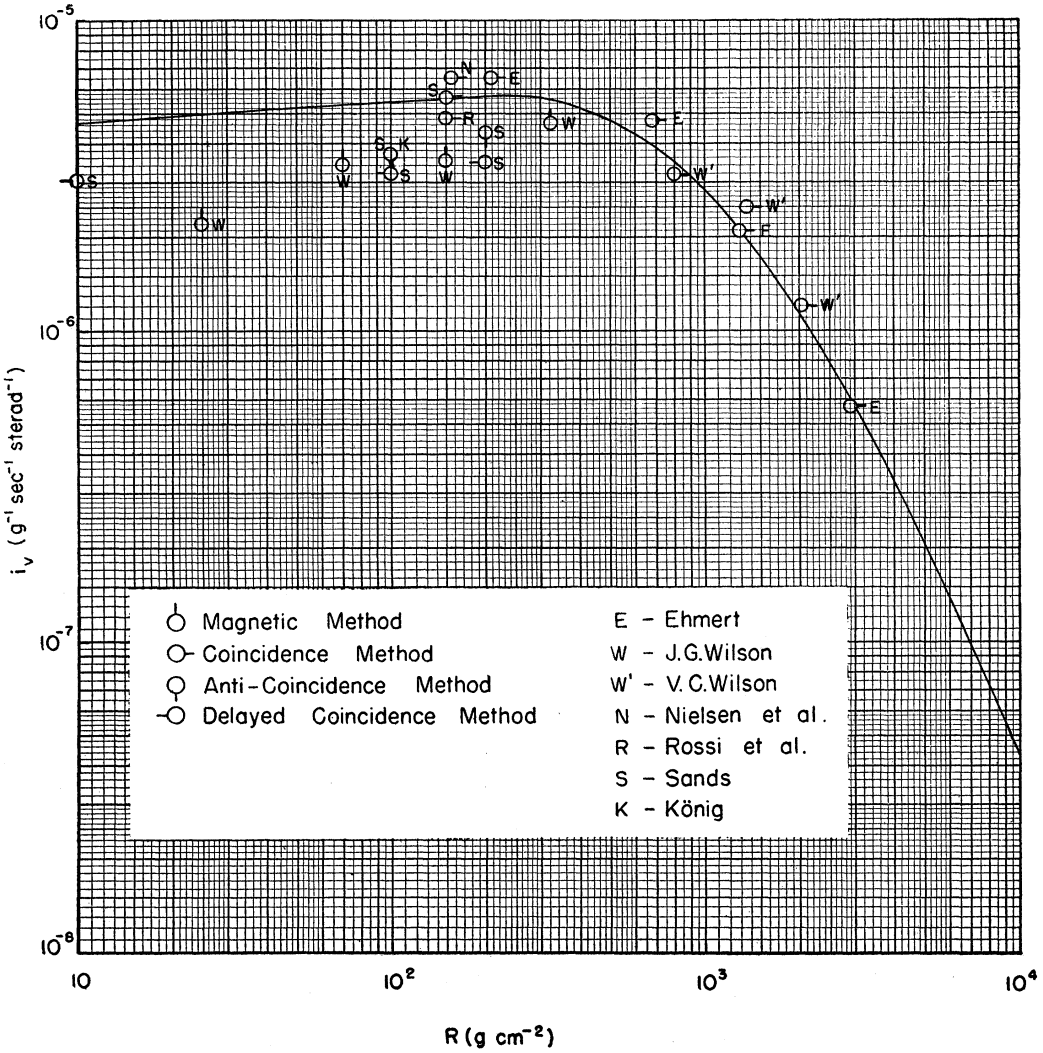

FIG. 6. Differential range spectrum of mesons at sea level. The range is measured in g cm^{-2} of air. The circles represent experimental data obtained by the following authors: Ehmert (E1), Koenig (K1), Nielsen *et al.* (N2), Rossi *et al.* (R4), Sands (S3), J. G. Wilson (W7), V. C. Wilson (W8).

depths under water and under ground, respectively, by means of cosmic-ray telescopes with no lead between the Geiger-Mueller counters (see also the work of Clay C2; C3). When plotted against equivalent absorber thickness and normalized at one depth, the data of Ehmert and Wilson fall on a single curve, which is reproduced in Fig. 5. Equivalent absorber thicknesses of different materials are considered to be those corresponding to the ranges of mesons of the same energy in the two materials. The horizontal scale in Fig. 5 represents thickness of the absorber above the counters, from sea level, in g cm^{-2} of air equivalent. A lead thickness of 167 g cm^{-2} corresponds to an air thickness of 100 g cm^{-2}. Accordingly, the vertical scale in Fig. 5 is chosen so that the ordinate at 100 g cm^{-2} is equal to $0.83 \cdot 10^{-2}$, the accepted value of I_v for the hard component at sea level.

We will assume that the curve in Fig. 5 represents the integral range spectrum of mesons at sea level, i.e., that the ordinate of each point gives the number of mesons of range greater than the corresponding abscissa per centimeter-square second steradian. This assumption is justified by the following considerations: (a) The fractional

number of protons in the penetrating component is negligible. (b) The fractional number of electrons capable of traversing 100 g cm^{-2} of air is very small. Whatever electrons may be present under 100 g cm^{-2} and at greater depths must be for the most part the result of secondary processes of mesons, so that their number may be expected to be proportional to the number of mesons at all depths. This view is in agreement with Ehmert's finding that the percent decrease in counting rate caused by placing a 5-cm thick lead shield between the counters is the same at all depths, within the experimental errors.

Figure 6 shows the differential range spectrum i_v of mesons at sea level, i.e., the derivative with respect to R of the curve which gives the integral range spectrum. The quantity $i_v(R)d\omega$ represents the number of mesons which arrive at sea level in one second within the solid angle $d\omega$ in the vertical direction and are brought to rest in 1 gram of a light absorber after traversing a thickness R of the same absorber. It is measured in g^{-1} sec.$^{-1}$ sterad^{-1}. The experimental data used for the determination of the differential range spectrum are shown with circles in Fig. 6. Some of these data were obtained with the *coincidence* method; i.e., by taking differences between the counting rates of a cosmic-ray telescope with different absorber thicknesses above the counter. The accuracy of this method is limited by the fluctuations of the cosmic-ray intensity and by the statistical errors, both of which become important at the lower end of the range spectrum where one has to deal with small differences in absorber thickness.

The first source of error is eliminated and the second is greatly reduced by the use of anticoincidence methods, in which one measures directly the fractional number of particles that traverse a certain absorber thickness and are stopped by an additional (small) thickness. Some data obtained by this method are shown in Fig. 6. In determining the *absolute* value of i_v by the anticoincidence method one should apply corrections for scattering and for the effect of secondary electrons produced by the disintegration of those mesons which come to rest in the absorber. These corrections are very uncertain. Moreover, the coincidence and the anticoincidence methods fail completely for ranges smaller than about 100 g cm^{-2} of lead, where the number of electrons becomes important and where low energy protons may also be present in appreciable numbers.

In this region, the only usable method appears to be the method of the *delayed coincidences*, which makes use of arrangements similar to those employed in the measurements of the mean lifetime of mesons. In these arrangements, mesons after traversing a certain thickness of lead or other material are brought to rest in an absorber and subsequently decay into electrons which are detected by Geiger-Mueller counters surrounding the absorber. Some data obtained by this method are shown in Fig. 6. The method of delayed coincidences distinguishes unequivocally between mesons and other types of particles and its accuracy, as far as *relative* measurements are concerned, should be limited only by the statistical fluctuations. However, the determination of the absolute intensity of the differential range spectrum at any one point requires a computation of the probability for a decay electron, produced in the absorber, to be recorded. The accuracy with which this calculation can be made is very questionable, among other reasons on account of the uncertainty which still exists concerning the energy of the decay electron.

The curve in Fig. 6 represents what, on the basis of available data, appears to be the best estimate for the differential range spectrum of mesons at sea level. In drawing this curve, the data obtained from the method of delayed coincidences were used to determine the slope of the curve between 10 and 200 g cm^{-2}, while the evaluation of the absolute intensity was based on the results of the coincidence method for thicknesses greater than 150 g cm^{-2}.

If mesons lose energy only by collision phenomena, their distribution in range can be computed from their distribution in momentum (see Section 5) by making use of the theoretical momentum-range relation (see Appendix, Section 27). Some data obtained by this method (*magnetic* method) are plotted in Figs. 5 and 6, after normalizing the total number of mesons of momenta larger than 2 Bev/c to the intensity of the integral range spectrum at the corresponding range (920 g cm^{-2}). The agreement is very

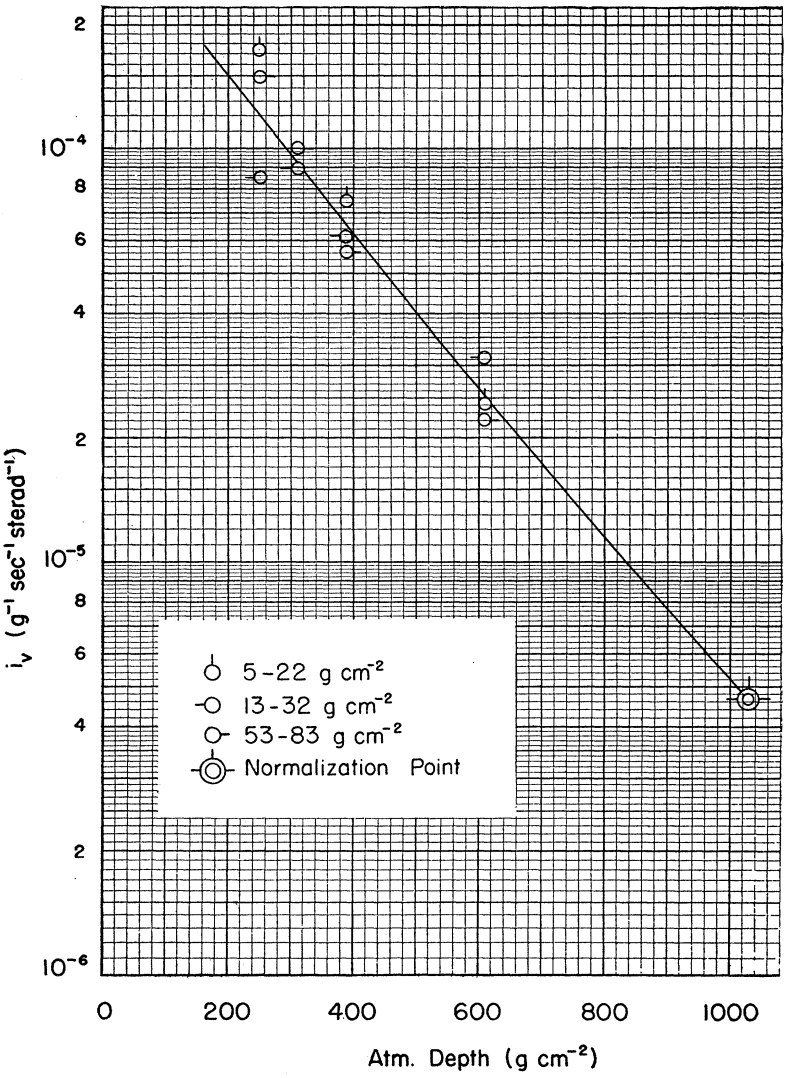

FIG. 7. Differential intensity of slow mesons as a function of atmospheric depth.

good in the range interval from 920 to 4000 g cm^{-2} (momentum interval from 2 to 10 Bev/c). The discrepancy at 8400 g cm^{-2} (20 Bev/c) is probably not very significant, on account of the large errors involved in the measurement of momenta as large as 20 Bev/c. Conceivably, the discrepancies at the low energy end of the spectrum may be due to the presence in the cloud-chamber experiments of a strong magnetic field which prevents some of the low energy particles from being recorded (even though this effect was taken into consideration and tentatively corrected for in Blackett's and Wilson's experiments).

7. Slow Mesons at Various Altitudes

The variation with altitude of the number of mesons near the end of their range was measured (R9; S3) with the method of the delayed coincidences (see Section 6). Three separate experiments were made in which the range intervals of the mesons recorded (for vertical incidence) were 5 to 22, 13 to 32, and 53 to 83 g cm^{-2} of air equivalent, respectively. No significant differences between the results of the three measurements were found, indicating that, within the experimental error, the differential range spectrum of mesons is flat between 5 g cm^{-2} and 80 g cm^{-2} at all altitudes. The counter arrange-

ment was such as to admit particles within a very wide solid angle around the vertical. Consequently, the quantity measured was more closely related to the integrated intensity than to the vertical intensity of slow mesons. Figure 7 represents the experimental data, normalized at sea level to the absolute value of the differential range spectrum of mesons at 10 g cm^{-2} as given in Fig. 6. The curve drawn through the experimental points will be interpreted as giving the number of mesons per second—steradian in the vertical direction which stop in one gram of air at the various depths. This interpretation is based upon the assumption that the angular distribution of slow mesons does not change appreciably with depth, an assumption which has not yet been tested experimentally.

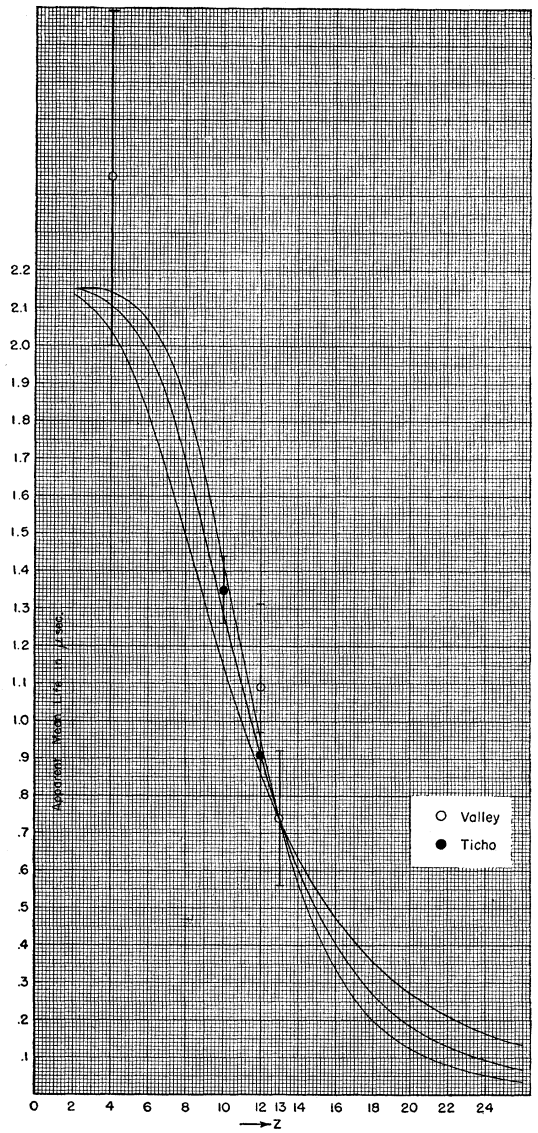

FIG. 8. Apparent lifetime of negative mesons as a function of the atomic number of the absorber. The experimental points were obtained with beryllium ($Z=4$), sodium fluoride ($Z_{Av}=10$), magnesium ($Z=12$), aluminum ($Z=13$). The three curves were computed under the assumptions that τ_c is proportional to Z^{-3}, Z^{-4}, Z^{-5}, respectively, and were normalized to the experimental value for aluminum at $Z=13$.

II. TRANSFORMATIONS OF COSMIC RAYS

8. General Considerations

The structure of cosmic rays changes gradually as they pass through matter by virtue of processes in which elementary particles and quanta disappear or are created and of other processes in which energy is transferred to electrons or nucleons originally at rest. These processes can be subdivided into three categories: electromagnetic interactions, nuclear interactions, and spontaneous disintegrations. The theory of electromagnetic interactions has been developed in detail from the general principles of quantum-electrodynamics and appears to represent the observed phenomena correctly. No well-established theory exists for the nuclear interactions or for the phenomena of spontaneous decay. The experimental data bearing on these two last classes of phenomena will be reviewed briefly in the following sections.

9. The Disappearance of Mesons

When mesons are brought to rest in an absorber, charged particles believed to be electrons are emitted from the absorber with time delays of the order of microseconds. (R1; M1; A4; R8; N1; C6; C7; C8; C9; C10; M2; S8; T3.) The delayed emission of electrons is observed only after the absorption of positive mesons when the absorber has a high atomic number; it is observed after the absorption of both positive and negative mesons when the absorber has a low atomic number (C7; C10; V1). The probability that an electron be emitted with a delay longer than t after the absorption of a *positive* meson is represented by an exponential law $\exp(-t/\tau^+)$. Within the experimental errors τ^+ has for all absorbers

the following value:

$$\tau^+ = (2.15 \pm 0.1) \text{ microseconds.}$$

The emission of electrons that follows the absorption of *negative* mesons in elements of low atomic number obeys a similar law, $\exp(-t/\tau^-)$. The time constant τ^-, however, has different values in different absorbers (T4; V2; V3; T5). In Fig. 8 the experimental values of τ^- that have been obtained so far are plotted against the atomic number Z of the absorber. It appears that τ^- is practically identical to τ^+ for $z \leq 4$ and decreases rapidly to a value small compared with one microsecond as Z increases from about 4 to about 20.

These results are interpreted by assuming that free mesons are unstable and have a natural lifetime against spontaneous decay given by

$$\tau = 2.15 \pm 10^{-6} \text{ sec.} \quad (6)$$

A positive meson, when stopped in an absorber, comes to rest at a large distance from the atomic nuclei because of electrostatic repulsion, and decays spontaneously with its natural lifetime. A negative meson, however, falls into a K orbit and the fact that in elements of intermediate atomic number τ^- is less than τ, while in elements of high atomic number no decay is observed, is attributed to the influence of the nearby nucleus. It has been suggested that the intense electric field existing in the proximity of the nucleus may shorten the natural lifetime of mesons (V2). A more likely hypothesis appears to be that mesons are captured by atomic nuclei. If τ_c represents the characteristic lifetime for this capture process, then the competition between decay and capture reduces the apparent lifetime of negative mesons to a value τ^- given by the equation

$$1/\tau^- = (1/\tau) + (1/\tau_c). \quad (7)$$

Since the radius of the meson K orbit is inversely proportional to the atomic number Z, the density of the meson wave function at the nucleus is proportional to Z^3. On the other hand, the capture probability is proportional to the density of the meson wave function at the nucleus and to the number of nucleons in the nucleus, which, for light elements at least, is approximately proportional to Z. Hence τ_c should vary as Z^{-4} (W1). The curves plotted in Fig. 8 represent τ^- as a function of Z computed from Eq. (7) under the assumptions that τ^- varies as Z^{-3}, Z^{-4}, and Z^{-5}, respectively. The curves are fitted to the experimental data at $Z=13$. It appears that the experimental results so far obtained are consistent with the fourth-power law, but are not precise enough to establish its validity.

If the capture hypothesis is correct, a relation should exist between the apparent lifetime of negative mesons, τ^-, and the fractional number of the absorbed negative mesons which undergo decay. This quantity, in fact, is given by the expression

$$f = \tau^-/\tau. \quad (8)$$

Experiments are in progress to determine f for aluminum. The results so far obtained are not sufficiently accurate to prove or disprove the capture hypothesis.

Mesons in flight, both positive and negative, are assumed to decay with their characteristic lifetime τ. It is believed that this phenomenon is responsible for the anomalous absorption of mesons in the atmosphere; in fact, the observation of this phenomenon furnished the first indication of the radioactive instability of mesons. It may be pointed out, however, that some difficulty seems to exist in explaining the anomalous absorption *quantitatively* on the basis of the value for τ given by (6) and of the most reliable determinations of the meson mass.

10. The Products of the Disappearance of Mesons

Very little information is available as yet on the products of the disintegration of mesons. The conservation principles of energy and momentum require that at least two particles be produced when a meson decays. If only two particles are produced, they go off with equal and opposite momenta in the frame of reference in which the meson was at rest. Because of the principle of conservation of electric charge, one of the two particles must be charged and since it must have a mass smaller than the meson mass, it must be either an electron or a particle of mass intermediate between those of the electron and the ordinary meson.

There are experimental results showing that, ordinarily at least, when a meson stops in an absorber only *one* charged particle is emitted (W3; A2; V3). There is also some experimental evidence showing that the decay of mesons is ordinarily *not* accompanied by the emission of photons (H4; S4). If each meson disintegrates into one electron and one neutral particle, then the decay electron should always have the same energy in the frame of reference in which the meson is at rest. If the neutral particle is a neutrino, the electron energy should be almost exactly one-half the rest energy of the meson, i.e., 50 Mev. If the neutral particle is considerably heavier than an electron (neutretto) the energy of the decay electron should be correspondingly smaller. If more than one neutral particle is produced, then the decay electrons should exhibit a continuous energy distribution, and the average value of their energy should be smaller than 50 Mev.

Only two cloud-chamber pictures have been published so far in which one sees a meson stop in the gas of the chamber and produce what appears to be a decay electron, the momentum of which can be measured by the curvature of the track in a magnetic field. One of the pictures (W3) gave an electron energy of about 70 ± 35 Mev in fair agreement with the hypothesis of the disintegration into an electron and a neutrino. The second picture (A2) gave an electron energy of 24 Mev, which would rather favor the hypothesis of the disintegration into an electron and a neutretto, or into an electron and several neutrinos.[1] To this very scarce cloud-chamber information one may add the results of some absorption experiments of Conversi and Piccioni (C9), which indicate that the range of the decay electrons cannot be much shorter than the computed range of a 50-Mev electron. The only conclusion is that more experiments are necessary before one can determine with confidence the nature of disintegration products of mesons.

A very obscure problem is what happens to the rest energy of those negative mesons, which in elements of intermediate or high atomic number seem to disappear otherwise than by the normal disintegration process. If a meson is captured by a nucleus, one would expect the nucleus to disintegrate as a result of the energy released in it by the disappearance of the meson. No cloud-chamber pictures showing nuclear disintegrations at the end of meson tracks have been reported so far, and it has been pointed out by Piccioni (P3) that, if such phenomenon did occur, it would hardly have escaped detection. Nuclear disintegrations at the end of meson tracks were found in photographic emulsions (P1; O1; L2). It is likely, however, that the mesons responsible for these phenomena are not ordinary mesons, but rather "heavy" mesons.

The possibility that nuclei after absorbing a negative meson lose their excitation energy by γ-ray emission (either directly or through the intermediary of a hypothetical short-lived meson) is being tested by Piccioni. His preliminary results indicate that no high energy γ-rays are produced when mesons come to rest in iron (P3).

11. Interactions of Mesons with Matter

The study of the passage of mesons through matter has so far failed to establish with certainty the existence for mesons in flight of any nuclear interaction, i.e., of any interaction which cannot be explained by electromagnetic phenomena.

Direct cloud-chamber measurements of momentum losses of penetrating particles in metal plates by Ehrenfest (E2) and by Wilson (W4; W5), as well as the comparison between the momentum spectrum and the range spectrum of penetrating particles at sea level discussed in Section 6, show that if mesons undergo any momentum loss by nuclear interactions, the average value of this loss is certainly small compared with the momentum loss by collision with electrons.

Nuclear collisions may be expected to give rise to large angle scattering and to reactions in which high energy protons and mesons are produced. Cloud-chamber observations of the passage of several thousands of cosmic-ray particles through metal plates at *sea level* show that phenomena of this kind are extremely rare. For instance, Wilson (W6) found only one case of nuclear interaction leading to proton emission for a total thickness of 50 meters of lead equivalent traversed by pene-

[1] One more somewhat doubtful picture which seems to show a 24-Mev decay electron was presented by Anderson at the January meeting of the American Physical Society in New York.

trating particles. Three such cases were detected by Brode and Starr (B11) in an experiment in which about 200 meters of lead equivalent had been traversed by penetrating particles. Fretter (F3) did not find a single case of nuclear disintegration by penetrating particles over a path of 180 meters of lead. Code (C4) observed the passage of about 450 penetrating particles through 3.8 cm of tungsten (total equivalent lead thickness: 30 meters). He did not find any case of nuclear disintegrations, but found a few cases of large angle scattering which are difficult to explain by Coulomb interaction. From this very meager experimental data and under the assumption that the penetrating particles undergoing nuclear interactions are mesons, one estimates a cross section between 3 and $7 \cdot 10^{-27}$ cm^2 per nucleus of lead for meson interactions leading to high energy nuclear disintegrations or to large angle scattering. On the other hand, this cross section may well be much smaller and even zero because it is likely that most, and it is possible that all, of the observed nuclear interactions are produced by high energy protons.

Some experiments indicating that part of the small angle scattering of mesons in matter is caused by phenomena different from Coulomb interaction, have been reported by Sinha (S9) and Shutt (S7). The evidence, however, does not appear to be completely convincing. In any case, this phenomenon, interesting as it may be on its own merit, would not affect appreciably the behavior of mesons. Thus we feel justified in disregarding nuclear interactions of ordinary mesons in the general description of cosmic-ray phenomena.

12. Stars and Penetrating Showers

A number of observations have brought to light several secondary cosmic-ray phenomena which clearly indicate the existence of nuclear interactions. Among such observations are the following:

(a) *Cloud-chamber pictures of "stars."*—(See, among others, D1; H2; P4.) By expanding cloud chambers at random, pictures are occasionally obtained which show groups of heavily ionizing particles diverging at wide angles from a point in the gas, in the walls of the chamber, or in whatever solid material may be present inside the chamber. Any such group of particles, whether or not accompanied by fast, lightly ionizing particles, will be described as a "star." Often the tracks can be recognized as those of protons, of α-particles, or of heavier nuclear fragments. The number of particles traveling upward seems to be comparable to that traveling downward. The energies of the individual star particles are of the order of 10^6 or 10^7 ev. The phenomenon is interpreted as a nuclear explosion requiring an energy transfer of the order of 10^8 ev or of a small multiple of this quantity from an external agent to a nucleus. In most pictures, no track of a fast ionizing particle is visible in the picture, and it is thus concluded that most stars are produced by non-ionizing rays. According to Hazen the rate at which pictures of stars are obtained is about 5 times greater at 4300-meters than at 3000-meters altitude.

(b) *Cloud-chamber pictures of "penetrating showers."*—(See, among others, F2; J2; S7; P4; H1; R3.) Some cloud-chamber pictures show groups of lightly ionizing penetrating particles diverging in a general downward direction from a common point located either outside or inside the cloud chamber (however, no picture of a group of particles originating in the gas has been reported so far). These groups of particles will be called "penetrating showers." The particles of a penetrating shower from their specific ionization appear to be singly charged and to have relativistic velocities. A few of them were recognized as protons, a few others as mesons. However, in the majority of the cases their nature could not be determined, so that the proportion of mesons and protons in the penetrating showers is not known. Also, perhaps with one or two exceptions (H1; R3), it has not been possible to establish that the mesons in penetrating showers are ordinary mesons. Occasionally, low energy protons, α-particles, or heavier nuclear fragments are seen to originate from the same center as the high energy penetrating particles, indicating that sometimes at least the production of penetrating showers is accompanied by nuclear disintegrations. Even if this is always the case, as appears likely, the low energy products of the disintegrations will be detected only seldom, namely, when the radiating point happens to be separated from the sensitive

volume of the chamber by a very small absorber thickness. A penetrating shower is interpreted as a reaction in which mesons are produced and the nucleus explodes into a number of low energy fragments and a few high energy nucleons. The energy transfer required for such a phenomenon is of the order of 10^9 ev or more. Penetrating showers seem to be produced in comparable numbers by ionizing and by non-ionizing rays. Pictures of penetrating showers were obtained both with random expansions and with expansions controlled by Geiger-Mueller counters arranged so as to favor the recording of this particular event. With random expansions, stars appear more frequently than penetrating showers.

(c) *Stars in photographic emulsions.*—Nuclear explosions, of the same type as those which are responsible for the cloud-chamber pictures of stars, are presumably the origin of the "stars" which are found in the microscopic examination of photographic emulsions. In general, high energy nuclear events cannot be distinguished from those of low energy by the photographic method because particles of relativistic velocity do not leave detectable tracks in the emulsion and, therefore, in both cases only the low energy protons and nuclear fragments are usually detected. The recent improvements of the photographic technique, however, have made it possible to detect the production of *low energy mesons* in nuclear explosions (L1; L2).

The rate of production of stars increases rapidly with height. According to the recent experiments of Perkins (P1), the increase is by a factor of 10 from sea level to 3600-meters and by another factor of 2 from 3600-meters to 4300-meters This corresponds to an approximately exponential dependence on atmospheric depth with an "absorption thickness" of about 135 g cm^{-2}.

13. Ionization Bursts

The observation of "bursts" in ionization chambers provides a convenient method for studying the variation in the rate of occurrence of nuclear reactions as a function of altitude or of other parameters. In a thin-walled unshielded ionization chamber, bursts can be produced by the passage through the chamber either of a large number of electrons from an air shower or of a small number of heavily ionizing particles from a star. The two phenomena can be separated by recording simultaneously the pulses of two or more ionization chambers arranged close to one another. Air showers will produce pulses of comparable size in all chambers while nuclear disintegrations will produce mostly pulses in single chambers, occasionally pulses in two, and very seldom in more than two chambers. Moreover, multiple pulses produced by nuclear disintegrations will be usually of unequal sizes. By this method it was shown by Rossi and Williams (R10) that at 3500-meters altitude about 98 percent of the pulses, corresponding to an energy loss of more than 6 Mev in a thin-walled cylindrical ionization chamber of about 2-liter volume and filled with argon at 5-atmosphere pressure, are caused by nuclear disintegrations and only 2 percent by air showers. The characteristics of the chamber and the bias are here explicitly stated because the number of bursts produced by showers relative to the number of bursts produced by nuclear disintegrations increases greatly as the gas pressure or the bias is increased.

Some preliminary results on the rate of occurrence of bursts at various altitudes are presented in Fig. 9. These results were obtained by the following experimenters: Bridge (B7; B9) and Williams (R10) on the ground (both at sea level and at various altitudes in the mountains); Bridge (B7) in an airplane; Hulsizer (H6) with balloon-borne equipment; Tatel and Van Allen (T2) with chambers installed in the warhead of a rocket. All of the experiments with the exception of Hulsizer's were made with two-liter cylindrical chambers of the type described above. The chamber used in Hulsizer's balloon measurements was of similar design but of smaller dimensions. With this chamber measurements were taken also at 9000-meter altitude aboard an airplane, and the results were used to normalize the data to those obtained by Bridge at the same elevation.

As already pointed out, at 3500 meters only a very small fraction of the bursts observed are caused by air showers. On the other hand, in the lower part of the atmosphere, the variation with altitude in the rate of occurrence of air showers of the particle density required to produce the observed pulses does not seem to differ greatly from the variation with altitude in the rate of occur-

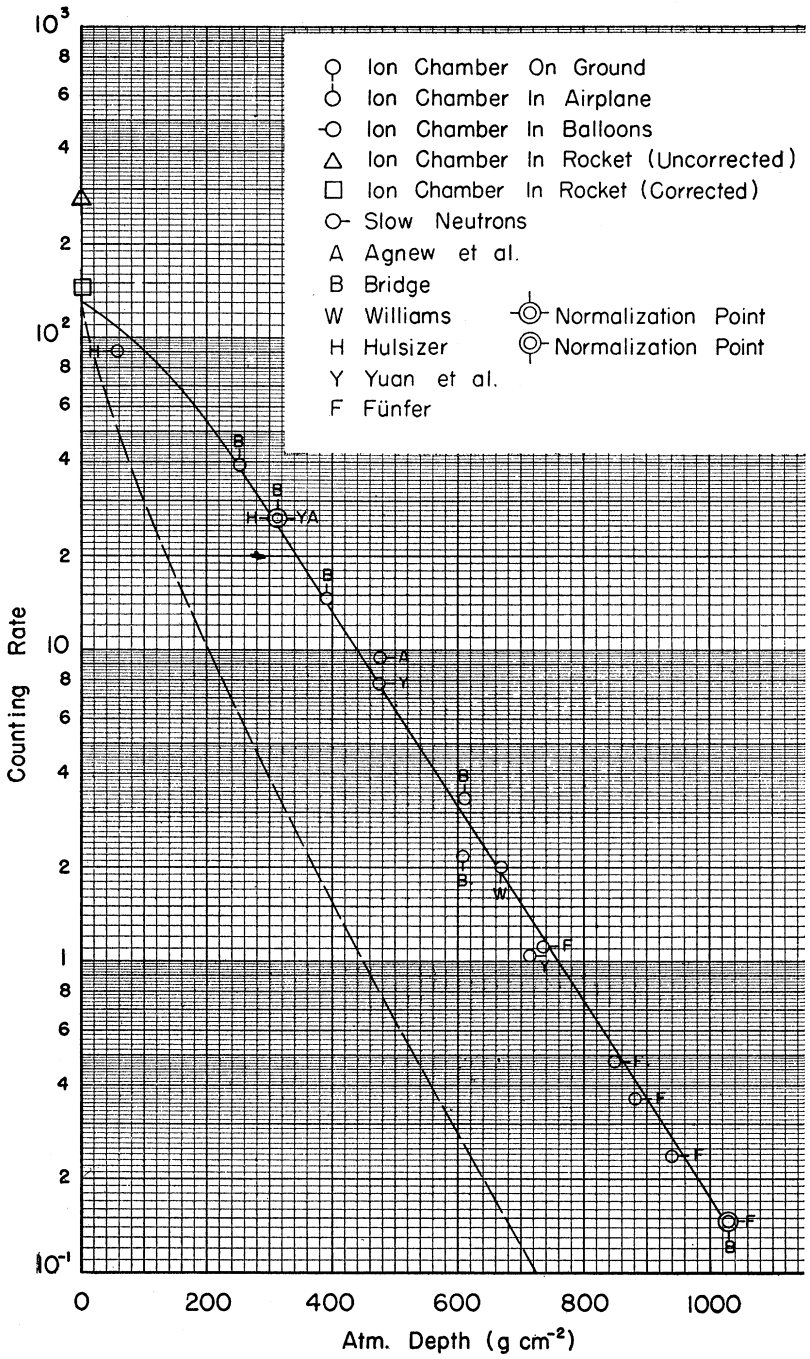

FIG. 9. Counting rates of unshielded ionization chambers and of slow neutron detectors at different atmospheric depths. All the data are normalized to the counting rate per minute of a cylindrical ionization chamber 7.5 cm in diameter, 52 cm long, filled with argon at 5 atmospheres pressure and biased at 8 Mev. For the slow neutron data of Agnew *et al.* and of Yuan *et al.* the normalization point is at 310 g cm^{-2}. For the slow neutron data of Fünfer the normalization point is at 1030 g cm^{-2}. The straight portion of the solid line represents the exponential function $\exp(-x/138)$. The broken curve represents the function $\exp(-x/138) + (x/138)E_i(-x/138)$.
Note: It the ordinate scale 10^{-1}, 10, 10^2, and 10^3 should read 10^{-2}, 1, 10, and 10^2, respectively.

rence of bursts, while beyond 5000 meters, air showers increase less rapidly than bursts with increasing altitude (K2). Thus, it is safe to assume that the contribution of air shower to the burst rates shown in Fig. 9 is small at all altitudes. In the rocket experiments, however, it is likely that an appreciable number of bursts were produced by showers generated in the heavy material which, in these experiments, was present in the neighborhood of the chambers. Since four chambers were used, it is possible to discriminate against these events by rejecting all cases in

which two or more chambers exhibit pulses of comparable size. The same selection rule can be applied to the measurements carried out by Williams at 3500 meters with four chambers of the same type. One then finds that the bursts so selected increase by a factor of 73 from 3500 meters to a point outside the atmosphere. This result is shown by the square in Fig. 9. Below 10,000 meters, the curve of the burst rate *vs.* depth is represented within the experimental errors, by the law $\exp(-x/L_a)$ with $L_a = 138$ g cm^{-2}. This absorption thickness is not appreciably different from the one which represents the altitude dependence of the rate of production of stars in photographic plates.

The data shown in Fig. 9 refer to ionization pulses larger than 8 Mev. It may be noted that *approximately* the same curve is obtained for all bias settings between 5 and 10 Mev, at least for depths larger than 250 g cm^{-2}.

14. Protons, α-Particles, and Neutrons of Low Energy

Cloud-chamber observations and examination of photographic emulsions reveal the existence in the atmosphere of a certain number of slow protons and α-particles, which seem to have an approximately random directional distribution.

According to Perkins (P1), between sea level and 4300 meters the number of single tracks in photographic emulsions increases with altitude at the same rate as the number of stars.

It is natural to assume that the observed slow protons and α-particles are produced in nuclear interactions of the same kind as those which give rise to the stars in the photographic emulsions. Under this assumption, the ratio of the number of single tracks to the number of stars can be calculated from the observed range distribution of star particles and the average number of particles per star. It is stated by Perkins that the results of this calculation are in agreement with the experimental data. The fact that the ratio of single tracks to stars is approximately the same at sea level and at 4300 meters indicates that neither the average number of particles per star nor the range distribution of the star particles changes appreciably between these two altitudes.

Another cosmic-ray effect presumably connected with nuclear disintegrations is the presence in the atmosphere of neutrons with thermal and epithermal velocities. These neutrons are usually detected by means of boron counters. Since the cross section for the boron (n, α) reaction is inversely proportional to the neutron velocity, we may assume that the counting rate of a boron detector is a measure for the *density* of slow neutrons.

Most of the observed neutrons are probably produced with energies of the same order of magnitude as the ionizing star particles; i.e., with energies of about 10^7 ev. They are then slowed down, first by inelastic collisions, then by elastic collisions with atomic nuclei in air, until eventually they are captured by nitrogen through an (n, p) process. According to Bethe, Korff, and Placzek (B4), the average distance traveled by a neutron from the place of production to the place of absorption is of the order of 150 g cm^{-2}. Thus at distances from the top of the atmosphere large compared with 150 g cm^{-2} the slow neutron density should vary as the rate of occurrence of nuclear disintegrations. This is borne out by experiments, as shown in Fig. 9 where the slow neutron data obtained by Funfer (F4), by Agnew, Bright, and Froman (A1), and by Yuan and Ladenburg (Y2) are plotted along with the data on burst production in thin walled ionization chambers.

15. Production of Electronic Radiation in Nuclear Interactions

Some of the electrons and photons in the atmosphere arise from the decay of ordinary mesons and from electromagnetic interactions of these particles with matter (mainly collision processes). However, definite experimental evidence has been obtained recently for the production of electronic radiation in processes of a different kind, which appear to involve nuclear interactions.

Cloud-chamber pictures have been reported which show the simultaneous appearance of stars and electronic tracks (D1). Other cloud-chamber pictures have been published in which one sees showers containing both electrons and penetrating particles (F2; B10).

In another type of experiment (B8) an ionization chamber was placed some distance below a tray of Geiger-Mueller counters and a 15-cm

thick lead shield was placed between the two instruments (see Fig. 10A). Some of the pulses from the ionization chamber were found to be time-coincident with pulses from the Geiger-Mueller tray and were interpreted as caused by electronic showers produced in the lead by ionizing particles coming from above. These particles cannot be electrons because electrons capable of producing showers of the observed size (35 particles or more) through 15 cm of lead must have an energy of at least 10^{12} ev and electrons of this high energy are too scarce to account for the observed coincidence rates. The possibility that the observed showers may be produced by ordinary mesons through collision or radiation processes is ruled out by the altitude dependence of the effect. Some preliminary experiments (B8) showed that the coincidence rate increases by a factor of several hundreds from sea level (1030 g cm^{-2}) to 9000 meters (310 g cm^{-2}). For the same altitude interval the total penetrating component increases only by a factor of 6 and presumably the number of mesons with sufficiently large energy to produce collision or radiation showers of the observed size increases by an even smaller factor. (Further data on the altitude dependence of burst production by penetrating particles are given in Fig. 12.)

A more detailed study of the shower production by penetrating particles was made with the experimental arrangement shown in Fig. 10B (B10). The cloud chamber contained eight $\frac{1}{4}$-in. lead plates and was triggered by the coincidences between the Geiger-Mueller tray and the ionization chamber. A number of pictures were obtained which show electron showers initiated in the lead plates by penetrating particles. Some of the showers were quite large and implied a lower limit of the order of 10^{10} ev for the energy of the penetrating particle from which they originate. Two-thirds of these pictures showed penetrating particles, and/or stars associated with the electron showers. Occasionally, one of the penetrating particles could be identified as a meson. In the remaining one-third of the pictures the density of the electron shower was so great as to make it impossible to detect penetrating particles if any were present. In order to obtain more information on the penetrating component of the showers, the experiment was rearranged as shown in Fig. 10C. The purpose of the lead between the ionization chamber and the cloud chamber was to filter out the electronic radiation. A large fraction of the pictures taken with this arrangement showed penetrating particles. Thus the experimental results are consistent with the assumption that penetrating particles are always produced in the nuclear events which give rise to electron showers. On the other hand, it is still uncertain whether or not penetrating showers are always accompanied by electronic radiation. The fact that in a large fraction of the pictures of penetrating showers no electron tracks are visible does not provide crucial evidence against production of electrons because the electronic part of a shower is much more readily absorbable than the penetrating part and, therefore, will be detected only if the center of radiation is not located too far inside the absorber.

16. Hard Showers

Coincidences are occasionally observed between Geiger-Mueller counters placed out of line and separated by large thicknesses of lead. Janossy (J1) has shown that the cosmic-ray events responsible for these coincidences cannot be identified with ordinary cascade showers. These events will be referred to as *hard showers*. Two typical arrangements for the observation of hard showers are shown in Fig. 11.

The nuclear interactions responsible for the production of hard showers are presumably of the same type as those discussed previously in which penetrating particles are generated either alone or in conjunction with electronic radiation. One

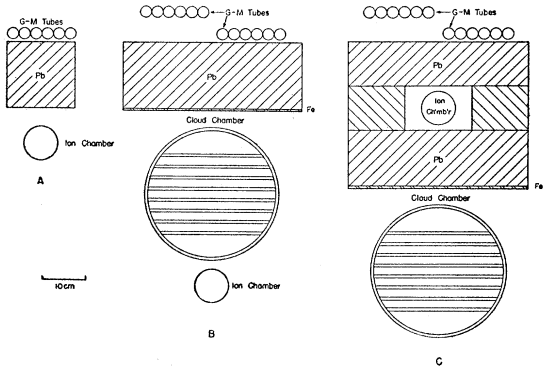

FIG. 10. Experimental arrangements for the investigation of shower production by penetrating particles.

has to keep the possibility in mind that some of the particles arising in these nuclear interactions may be capable of producing further nuclear interactions. If this is the case, such multiple interactions may play an essential role in the production of hard showers on account of the very large amount of material which surrounds the Geiger-Mueller counters. No detailed discussion will be given here of the many experimental results concerning hard showers which were obtained by Janossy and his collaborators. We shall only mention that the rate of occurrence of hard showers has been found to increase rapidly with decreasing atmospheric depth. Janossy and Rochester (J5) investigated the barometric effect of hard showers and found a 10 percent increase in the shower rate for 1-cm Hg decrease in atmospheric pressure. Some preliminary data on the altitude variation of hard showers obtained recently by Tinlot (T6) are shown in Fig. 12. These data as well as the barometric effect are consistent with a dependence on depth of the form $\exp(-x/L_a)$ with $L=125$ g cm^{-2}. A similar rate of increase of counting rate with decreasing atmospheric depth was obtained by Sala and Wataghin (S1) with an arrangement designed to favor the recording of hard showers coming from the air rather than those generated locally.

Some data on burst production by penetrating particles at various altitudes, obtained by Bridge (B9) with the equipment shown in Fig. 10A, are included in the graph of Fig. 12. There seems to be some indication that burst production increases with altitude somewhat more rapidly than hard showers, but the difference is not outside of the experimental errors.

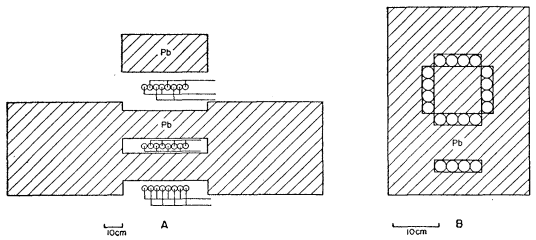

FIG. 11. Two experimental arrangements for the study of hard showers. *A* (J3); a record is obtained whenever one counter in each of the seven groups shown in the diagram is discharged. *B* (T6): a record is obtained whenever any two counters in each of the three horizontal trays is discharged. (The two vertical trays shown in the figure can be used to provide supplementary information on the structure of the showers.)

17. Origin of the Nuclear Events. The *N*-Component

It is possible that all kinds of rays, provided they possess sufficiently high energies, are capable of producing nuclear reactions of the types described in the preceding sections. It appears certain, however, that the cross section for nuclear interactions is very different for the different types of rays. It is thus convenient, from a phenomenological point of view, to consider the rays which are mainly responsible for the nuclear events as forming a separate component of the cosmic radiation, which, for the sake of brevity, will be called the *N*-component. The question then arises as to the nature of this component.

(a) *Mesons in the momentum range from $3\cdot10^8$ to 10^{10} ev/c.*—These particles form the bulk of the hard component of cosmic rays at sea level. Since all nuclear effects increase with altitude much more rapidly than the hard component, one concludes that not more than a negligible fraction of the nuclear events of any kind observed at high altitudes can be produced by mesons in the momentum range specified above.

(b) *Mesons of momentum less than $3\cdot10^8$ ev/c.*—These mesons cannot produce high energy nuclear reactions but might conceivably produce reactions of comparatively low energy, for instance, stars. In fact it has been often suggested that most of the stars may be produced by nuclear absorption of ordinary negative mesons. This hypothesis is disproved by the fact that, as already mentioned, no cloud-chamber evidence for such an effect exists. Actually, in most cloud-chamber pictures of stars no track is visible that could possibly be attributed to a slow meson. Moreover, the number of slow mesons increases with altitude less rapidly than the number of stars.

(c) *Mesons of momentum larger than 10^{10} ev/c.*—The possibility that mesons of very high energy may be responsible for a large fraction of the nuclear events cannot be ruled out. One would have to assume that the cross section for nuclear interactions is so large as to determine a fast absorption of these mesons in the atmosphere.

(d) *Electrons and photons.*—The following experimental evidence shows that electrons and photons do not play an important role in the production of nuclear events.

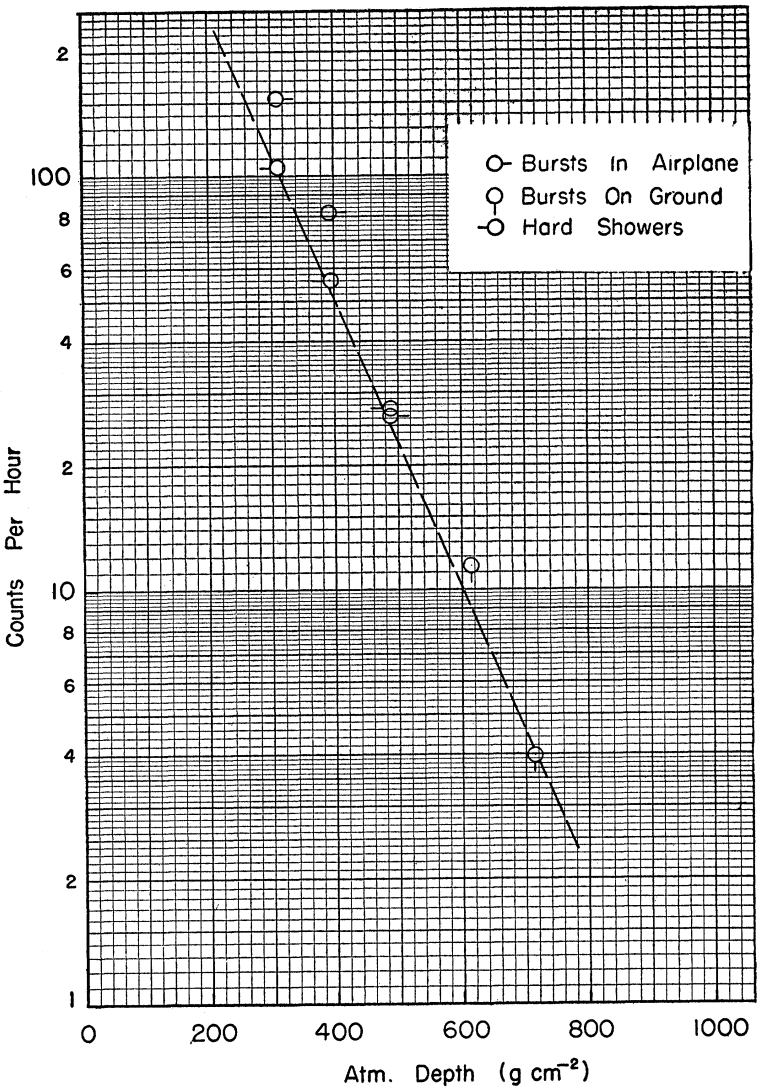

FIG. 12. Hard showers and burst production by penetrating ionizing particles as a function of atmospheric depth. Hard showers were observed with the arrangement shown in Fig. 11B; the counters were 2.5 cm in diameter, 25 cm long. Burst production by penetrating particles was observed with the arrangement shown in Fig. 10A; the counters were 2.5 cm in diameter, 50 cm long; the chamber was 7.5 cm in diameter, 52 cm long; it was filled with argon at 5 atmospheres pressure and was biased so as to record pulses larger than 3.2 Mev. Ordinates are actual counts per hour.

(1) With a cloud chamber operated under lead, one obtains pictures of stars and of penetrating showers which do not show any electron tracks. The probability of a high energy photon emerging from a lead shield unaccompanied by a shower of electrons is extremely small.

(2) The analysis of photographic plates exposed under thick lead shields shows that the star-producing radiation is not much weaker under lead than in the free atmosphere (P1).

(3) By means of a group of ionization chambers, arranged so as to make it possible to discriminate between showers and nuclear disintegrations (see Section 13), the absorption in lead of the radiation which produces the latter has been measured roughly (R10). It was found that about 30 cm of lead are necessary to reduce its intensity to 30 percent. The number of high energy electrons and photons under 30 cm of lead is certainly much less than 30 percent of their number in the atmosphere.

(e) *Protons and neutrons.*—It appears virtually certain that high energy nucleons play an important part in the observed nuclear events even though they may not be solely responsible for them. It is experimentally known that neutrons with energies near 10^8 ev exhibit a cross section for nuclear interactions of the same order of

magnitude as that indicated by the absorption of the N-radiation (H3). Moreover, if there is any truth in the current assumption that mesons are related to nuclear forces, one is led to the conclusion that where sufficient energy is available mesons must be produced in the interactions between two nucleons. The penetrating showers may well be the manifestation of such meson production processes.

(f) *New particles.*—It is possible that the N-component contains particles (charged or uncharged), different from electrons, protons, or ordinary mesons. Experimental evidence for the existence of such particles has been brought forward recently by Occhialini, Powell and their collaborators (L1; L2). The findings of these experimenters give some support to the assumption that these particles interact strongly with nuclei. They also point to the possibility that ordinary mesons do not arise directly in nuclear interactions, but as the disintegration products of heavier particles which, in turn, are produced in nuclear interactions.

Recently there has been much theoretical speculation concerning neutral mesons. It is possible, and even likely on theoretical grounds, that the electron showers which accompany nuclear interactions may arise from photons produced by the decay of short lived neutral mesons.

In conclusion, there appears to be very little doubt that what we have called the N-radiation consists to a large extent of high energy protons and neutrons and it is possible that it contains in addition new types of particles. If these particles have very short lives, it may be difficult to separate experimentally their effects from those arising directly in the nuclear interactions in which they are produced.

III. GENERAL DISCUSSION OF COSMIC-RAY PHENOMENA

18. The Primary Radiation

Through the study of the structure of cosmic rays, of the interactions of the various cosmic-ray components with matter, of the altitude, latitude, and directional dependence of different cosmic-ray effects, enough information has been obtained to justify an attempt to bridge the gaps in our knowledge with reasonable hypotheses and present a general picture of cosmic-ray phenomena.

For this purpose we consider first the experimental facts bearing on the nature of the primary cosmic radiation.

(a) It is known from the latitude effect that the primary cosmic radiation contains a large proportion of electrically charged particles with momenta between 4.5 and 15 Bev/c. The "knee" in the latitude curve shows that there are comparatively few particles if any with momenta below 4.5 Bev/c.

(b) From the East-West effect it is known that most, and possibly all, of the penetrating particles observed at altitudes between sea level and 9000 meters originate from positively charged primaries (J7; S5; Y1; S6).

(c) Ordinary mesons, on account of their short lifetime, cannot be part of the primary radiation.

(d) It appears from the altitude dependence of the phenomena discussed in Sections 12 to 16 that primary cosmic rays exhibit strong nuclear interactions as a consequence of which they are rapidly absorbed in the atmosphere. In fact no cosmic-ray effect can decrease with increasing atmospheric depth any faster than the primary radiation from which it originates, either directly or indirectly.

(e) It has been pointed out by Schein (S5) that there does not appear to be any large number of electrons or photons in the primary cosmic radiation. An experiment has been carried out recently to investigate this important question quantitatively (H6). A cylindrical ionization chamber 5 cm in diameter, 10 cm long, and covered with a 1-in. thick lead shield was sent to a high altitude by means of balloons. The ionization bursts greater than a certain size were recorded. This size was chosen to correspond to the ionization produced by 80 lightly ionizing particles traversing the chamber perpendicular to its axis. This is the average size of a shower generated in the lead shield by a 4.5-Bev electron or photon. At 27,000 meters (20-g cm^{-2} depth) 300 bursts per hour were detected. Comparison with the counting rate of an unshielded chamber indicates that probably fifty percent of these pulses were due to nuclear disintegrations in the walls or the gas of the chamber (see Section 13). If we assume that all of the bursts are produced by showers from

the lead and consider the geometry of the experimental arrangement, we obtain as an approximate upper limit for the integrated intensity of electrons and photons of energy above 4.5 Bev:

$$J_2 = 3 \cdot 10^{-3} \text{ cm}^{-2} \text{ sec.}^{-1} \quad \text{at} \quad x = 20 \text{ g cm}^{-2}.$$

Since 20 g cm^{-2} is about $\frac{1}{2}$ of a radiation length in air, the integrated intensity of high energy electrons and photons at the top of the atmosphere cannot be much greater than the value given above. On the other hand, the value of J_2 for the total incoming radiation is approximately 0.4 cm^{-2} sec.$^{-1}$ (see Section 25). Thus we conclude that not more than about one percent of the primary particles are electrons or photons with energies above $4.5 \cdot 10^9$. Actually, there is no need to assume the existence of any high energy electrons or photons in the primary radiation since the few showers observed may be produced by nuclear interactions of high energy protons (see Section 15). In any case, it can be considered as established that no major part of the cosmic-ray phenomena can be ascribed to high energy electrons or photons in the primary radiation.

The facts listed above favor strongly the conclusion that the primary cosmic radiation consists almost entirely of high energy protons (J7; S5). Indeed, the only alternative conclusions are: (a) that the primary radiation consists in part of nuclei heavier than the hydrogen nucleus, and (b) that there exist *stable* elementary particles other than electrons and protons. Unlikely as these alternatives may appear, they cannot be ruled out on the ground that such hypothetical components of the primary radiation have never been detected near sea level, as this may be a consequence of the rapid absorption in the atmosphere which is an established property of the primary radiation.

In the phenomenological approach to the cosmic-ray problem that we are following, we shall assume that *the primary radiation consists of positively charged particles, different from electrons and from ordinary mesons, which interact strongly with atomic nuclei.* Even though we believe that these particles are protons, we choose to denote them by the less specific name of *primary cosmic rays.* We then obtain the following broad picture of cosmic-ray phenomena. The primary cosmic rays interact with atomic nuclei as they penetrate the atmosphere. In these interactions the nuclei are disrupted and nucleons of various energies are emitted. In the same interactions, elementary particles are created which either are identical with ordinary mesons or disintegrate subsequently into ordinary mesons. Electrons and/or photons are also created, again either directly or through the intermediary of short lived mesons. The electronic component of cosmic rays arises partly from these electrons and/or photons, and partly from the decay and other secondary processes of ordinary mesons. The N-component consists of those primary particles which penetrate the atmospheric layer to the point of observation, of high energy nucleons released in nuclear collisions, and possibly of new particles (other than ordinary mesons) produced in these collisions.

19. Cosmic-Ray Phenomena Outside the Atmosphere

Cosmic-ray experiments have been performed recently by means of rockets at altitudes up to about 160 kilometers. The results obtained above the altitude at which the residual pressure is about 2.5 g cm^{-2} are considered as reflecting the properties of cosmic rays in the free space.

In some experiments, elaborate arrangements of Geiger-Mueller tubes and absorbers were used in an effort to measure the penetration and to study the secondary effects of the cosmic radiation outside the atmosphere. The results obtained by Golian and Krause (G2), which are in at least qualitative agreement with those of other experimenters, will be described here in some detail.

The equipment is shown in Fig. 13. Various combinations of coincidences and anticoincidences between the Geiger-Mueller counters were recorded. Some of the most significant results obtained are summarized in Table I. One or more numbers in a bracket indicate counters connected together as a tray. Sums of brackets signify coincidences between trays. A subtracted bracket indicates a tray in anticoincidence such that the discharge of any counter in that tray prevents the recording of the associated coincidence event.

It was found also that when an event of the type (1)+(3)+(6)+(7, 8, 9), (1)+(3)+(6)+(10, 11, 12), or (1)+(3)+(6)+(13, 14, 15) oc-

TABLE I. Counting rates recorded in free space with the counter arrangement shown in Fig. 13.

Event	Counts per minute
(1)+(3)+(6)	219
(1)+(3)+(6)−(2, 4, 5)	68
(1)+(3)+(6)+(10, 11, 12)	144
(1)+(3)+(6)+(13, 14, 15)	98
(1)+(3)+(6)+(13, 14, 15)−(2, 4, 5)	40

curs, often more than one counter in the trays (7, 8, 9) or (10, 11, 12) or (13, 14, 15) is discharged.

From an examination of these data the following facts stand out:

(a) The cosmic-ray particles observed outside the atmosphere have a large probability of producing secondary effects.

(b) When a coincidence occurs between counters of a vertical cosmic-ray telescope it is accompanied in more than 50 percent of the cases by discharges of counters placed outside of the beam defined by the telescope. Thus, with the experimental arrangement used, most of the coincidences between counters on a straight line are not caused by a single particle traversing the counters but rather by groups of particles arising in secondary processes. It is therefore difficult to obtain, from the observed coincidence or anti-coincidence rates, a value for the number of incident particles.

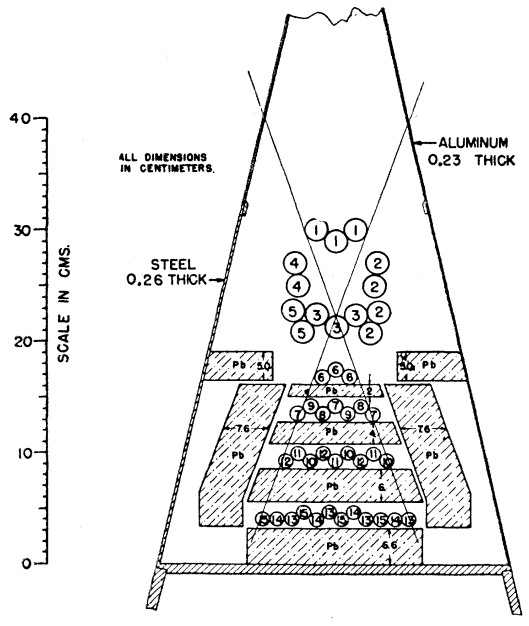

FIG. 13. Arrangement of G-M counters in the warhead of a rocket (from Golian and Krause G2).

(c) There is a large number of cases in which the unshielded counters of the telescope (1, 3, 6) are discharged while the shielded counters (10, 11, 12, 13, 14) are not.

Since there is no heavy material above the instrument, one must assume, in order to explain observation (b), that most of the secondary processes detected by the counter array take place in the lead shield. This shield is placed *below* counters 1, 2, 3, 4, 5. We conclude, therefore, that many of the secondary particles are produced at large angles with respect to the direction of the incident particles. The requirement of a large angular spread is somewhat mitigated by the fact that outside of the atmosphere the number of particles arriving at an angle from the vertical between θ and $\theta+d\theta$ with the vertical is proportional to $\sin\theta d\theta$. Thus a large proportion of the primary particles reach the instrument in nearly horizontal directions. The existence of nuclear cosmic-ray processes in which secondary particles are produced with large angular divergence is confirmed by some of the cloud-chamber pictures of penetrating showers. The arguments presented in Section 28 of the Appendix indicate that it is not unreasonable to expect large angles of emission even for particles of considerable energy if we assume that the nuclear interactions in which the secondary particles are produced can be described as collisions between two free nucleons.

Result (c) seems to indicate the existence in the radiation incident on the top of the atmosphere of particles which are stopped by moderate thicknesses of lead and do not produce any secondary particles capable of discharging Geiger-Mueller counters under the lead. Perhaps one should not accept this interpretation at face value. As Table I shows, in 80 percent of the cases in which counters 1, 3, 6 are discharged and 13, 14, 15 are not, there is a pulse in the side counters 2, 4, 5. It is therefore difficult to be sure that the comparatively few cases where 1, 3, 6 are discharged and neither 13, 14, 15 nor 2, 4, 5 are, actually represent particles crossing counters 1, 3, 6 and stopping in the 12 cm of lead between 6 and 13, 14, 15. If the interpretation is correct, however, one is led to the conclusion that many of

the particles observed at the top of the atmosphere are not primaries since it is difficult to see how a particle with sufficient energy to traverse the geomagnetic barrier can stop in 12 cm of lead without producing any secondary particles which emerge from under the lead. The presence of secondary particles at the top of the atmosphere can be understood if secondary particles are produced with a large angular spread. If a charged particle is projected upwards with a momentum smaller than the geomagnetic cut-off, the particle itself, or its charged disintegration products, will be brought back to the earth again by the earth's magnetic field. Thus, the secondary particles at the top of the atmosphere will travel in all directions, both upwards and downwards, except that no ordinary mesons or particles with comparable or shorter lifetime should be present in the downward stream. A theoretical estimate of the energy projected upwards is given in the Appendix (Section 29).

20. High Energy Nuclear Events

The N-radiation has been defined phenomonologically as that component of cosmic rays which is responsible for nuclear interactions. Therefore, any measurements of the rate of occurrence of nuclear events may be considered as a measurement of the intensity of the N-radiation. It is hardly necessary to point out that different methods of detection of the N-radiation weigh the various components of this radiation differently and are selective in a different manner to rays coming in the various directions. Thus, one should not be surprised if nuclear events of different kinds show a different altitude dependence. Indeed from the rate of occurrence of the various nuclear effects at various altitudes it should be possible to determine the variation with altitude of the total intensity, the composition, the energy distribution, and the angular dependence of the N-radiation.

The experimental data available to date are still incomplete so that whatever conclusions are reached at the present time will be necessarily of a preliminary nature.

We shall consider in this section the results of the observations on burst production by penetrating particles and on hard showers. Both of these phenomena are caused by high energy N-rays. In both types of experiments the probability of detection is greatest for vertical rays. The altitude dependence of these phenomena should therefore represent the altitude dependence of the vertical intensity of high energy N-rays. The experimental results, shown in Fig. 12, indicate that this intensity is an approximately exponential function of atmospheric depth and that the absorption thickness L_a is of the order of 125 g cm^{-2}.

The attenuation of the high energy component of the N-radiation with increasing atmospheric depth cannot be considered as a simple absorption process. In other words, we cannot assume that the N-rays present at a certain depth are all primary particles which have failed to undergo any nuclear collision in the air layer above. Indeed there is evidence that a large proportion of the high energy N-rays observed some distance below the top of the atmosphere are of a secondary nature, and are probably protons and neutrons released in nuclear collisions.

Cloud-chamber observations show that approximately equal numbers of penetrating showers are produced by ionizing and by non-ionizing rays (P4). The same is true for hard showers detected by counter experiments (J4). On the other hand (see Section 18), we believe that no appreciable number of neutral particles are present in the primary radiation.

The question then arises as to the relation between the absorption thickness L_a which determines the variation with depth of high energy N-rays and their collision thickness L_c which represents the average distance they travel before undergoing a nuclear encounter. For the moment, we can only say that L_a cannot be smaller than L_c. It may be, however, that L_a is appreciably larger than L_c. It is possible, for instance, that in a large fraction of the nuclear collisions, the N-particles lose only a small fraction of their energy. It is possible also that the propagation of the N-radiation through the atmosphere is a "cascade" phenomenon in which the absorption thickness depends on the energy spectrum of the radiation somewhat as in the case of electronic cascades, in which multiplication continues until the energy of the secondary particles fall below the "critical energy."

It is reasonable to assume, on theoretical

TABLE II. Tentative estimates of the numbers of protons in various energy ranges. It is assumed that the variation of these numbers with depth obeys an exponential law $\exp(-x/L_a)$ with $L_a=125$ g cm^{-2}. Momenta are measured in 10^8 ev/c; ranges in g cm^{-2} of air.

Quantity	Unit	Experimental information	Adopted sea level value
No. of particles $4<p<10$ $(6<R<100)$	cm^{-2} sec.$^{-1}$ sterad^{-1}	$\sim 10^{-2}$ at 9000 m (Anderson)	$3\cdot 10^{-5}$
No. of particles $10<p<30$ $(100<R<1000)$	cm^{-2} sec.$^{-1}$ sterad^{-1}	$\sim 7\cdot 10^{-4}$ at 9000 m (Anderson)	$2\cdot 10^{-5}$
Differential range spectrum i_v at $R=20$	g^{-1} sec.$^{-1}$ sterad^{-1}	$\sim 5\cdot 10^{-7}$ at sea level (Rochester)	$5\cdot 10^{-7}$
Differential range spectrum i_v at $R=100$	g^{-1} sec.$^{-1}$ sterad^{-1}	$\sim 4\cdot 10^{-7}$ at 1000 m (Leprince Ringuet)	$1.7\cdot 10^{-7}$

grounds, that the cross section for high energy nuclear interactions is at most equal to the geometric cross section of the nucleus, for which we can assume the approximate value:

$$\sigma=\pi(1.4\cdot 10^{-13})^2 A^{\frac{2}{3}}. \tag{9}$$

The collision thickness in air corresponding to the geometric cross section is 65 g cm^{-2}. Therefore we may place the following limits to the value of L_c:

$$65<L_c<125.$$

High energy protons are found both as part of the N-radiation and as one of the products of the interaction of high energy N-rays with matter. Therefore, we may expect their number to vary with depth as $\exp(-x/125)$. The very meager experimental information which is available at this time is consistent with the assumption that this is the case for protons of energy larger than about $\frac{1}{10}$ their rest energy, at least for depths between 250 and 1030 g cm^{-2}; and that, in the same depth interval, the shape of their energy spectrum does not change very drastically. In Table II we present the results of some very crude estimates of intensities, which are based upon the following experiments.

(a) Anderson (A3) has measured recently the momentum spectrum of positive and negative particles appearing single in a counter-controlled cloud chamber operated at 9000-meter altitude. He finds a much larger positive excess than at sea level and assumes that it is caused by protons. This interpretation is strengthened by the fact that the positive excess is found only for particles with momenta larger than about $4\cdot 10^8$ ev/c, which corresponds to the minimum momentum of a proton capable of traversing the amount of material between the sensitive volume of the chamber and the lower counter. From Anderson's measurements one can estimate that at 9000 meters the number of protons with momenta between $4\cdot 10^8$ ev/c and 10^9 ev/c is about 20 percent of the total number of "hard" particles at this altitude, and that the number with momenta between 10^9 ev/c and $3\cdot 10^9$ is about 15 percent.

(b) At 1000-m altitude, Leprince Ringuet (L3) found that 2.5 to 3 percent of the particles coming out of a 12-cm thick lead absorber with momenta between $3\cdot 10^8$ and $7\cdot 10^8$ ev/c are protons. If we convert from momenta to ranges, we obtain for the ratio of protons to mesons per unit range interval, at a range of 12 cm of lead, the approximate value of 6 percent.

(c) At sea level, Rochester and Bound (R2), using a cloud-chamber triggered by an anticoincidence arrangement which selected particles in a range interval of 2 cm of Pb (the lower limit of this interval being the thickness of the walls of the chamber and the counters, which is estimated as 10 g cm^{-2}), found certainly 8 and possibly 12 proton tracks in 372 hours of operation. If we consider the geometry of the experimental arrangement, we obtain for the number of protons in the range interval selected by the instrument the approximate value of $0.5\cdot 10^{-6}$ cm^{-2} sec.$^{-1}$ sterad^{-1}.

Very little is known on the behavior of high energy N-rays in materials other than air. Bridge has carried out some preliminary measurements at 4300 meters with an experimental arrangement of the type shown in Fig. 10A. The coincidence rate between the Geiger-Mueller tray and the ionization chamber was measured as a function of the lead thickness between the two instruments. The results obtained are shown in Fig. 14. The peak at about 3 cm is explained by shower production by electrons, the tail is attributed to shower production by high energy N-rays. From its slope an *absorption* thickness in lead of $L_a=280\pm 50$ g cm^{-2} is obtained.

With the arrangement shown in Fig. 11A, Janossy and Rochester (J3) have measured the rate of occurrence of hard showers as a function

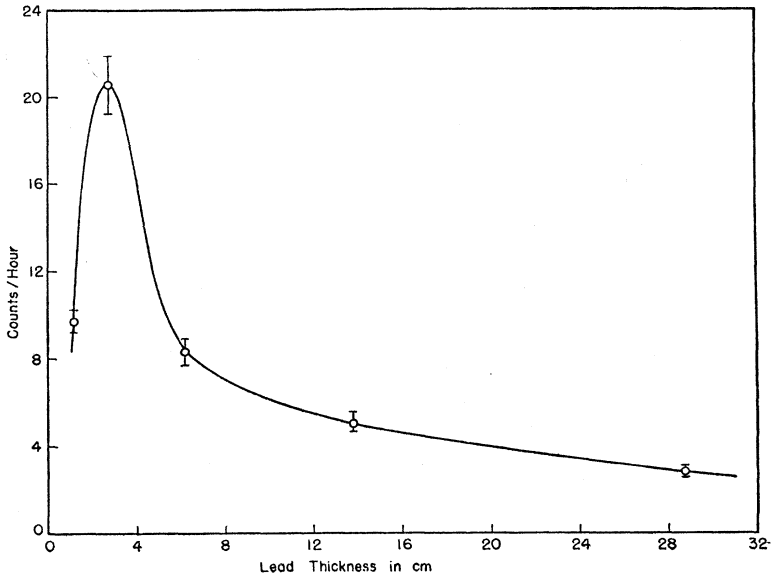

FIG. 14. Transition curve for burst production by ionizing particles obtained by Bridge (B9) with an experimental arrangement similar to that shown in Fig. 10A.

of the thickness of the lead shield placed above the top tray and have obtained the results represented in Fig. 15. The shape of the "transition curve" has been explained under the assumption that the coincidences observed are caused by showers of penetrating particles produced in the upper lead shield by a radiation for which the absorption thickness in lead is of the order of 5 cm. The results of the experiment of Bridge quoted above cast considerable doubt on this interpretation. It appears more likely that in many of the events described as hard showers the counters of the upper tray are discharged by electron showers produced simultaneously with penetrating particles. The thickness at which saturation sets in is then determined by the absorption of these electron showers rather than by the absorption of the primary radiation.

Rossi and Regener (R5) as well as Janossy and Rochester (J4) have found evidence for the production of penetrating particles by non-ionizing rays. The *collision* thickness of these rays, defined here as the mean thickness in which a collision leading to the production of secondary ionizing particles takes place, was found to be between 5 and 10 cm of lead. This result is not easily understandable because the collision thickness corresponding to the geometric cross section of lead nuclei is about 160 g cm^{-2} or 14 cm.

21. Low Energy Nuclear Events

Let us consider next the observations on stars and single tracks in photographic plates, on bursts in thin-walled unshielded ionization chambers, and on slow neutron effects. All of these phenomena are related to the production of particles of comparatively low energy in cosmic-ray induced nuclear disintegrations. They all appear to vary with altitude according to the same law, at least in the lower part of the atmosphere. As shown in Fig. 9, for depths larger than 250 g cm^{-2} this law can be approximated with the exponential function $\exp(-x/L_a)$ in which the absorption thickness L_a has the value of 138 g cm^{-2}. The minimum energy required for the production of the phenomena considered here

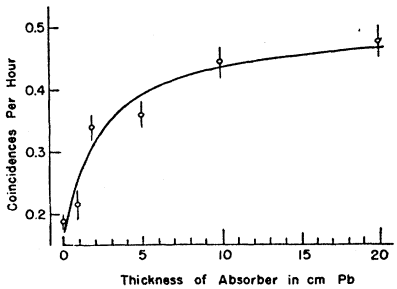

FIG. 15. Transition curve for hard showers obtained by Janossy and Rochester (J3) with the experimental arrangements shown in Fig. 11A. The abscissa is the thickness of the lead shield placed above the upper tray of counters.

is much smaller than the minimum energy required for the production of the phenomena considered previously. Moreover, the instruments used for their detection do not discriminate strongly in favor of any one direction. The curve in Fig. 9 may be considered therefore to represent the altitude dependence of the *integrated intensity* of N-rays of all energies. From an examination of this curve one can conclude that the nuclear disintegrations are not produced exclusively by a primary radiation which is absorbed exponentially by the atmosphere. In fact, if the intensity observed at an atmospheric depth x in a direction at an angle θ with the vertical is a function $I(x/\cos\theta)$, then the integrated intensity J_2 is related to the directional intensity I by equation

$$J_2(x)=2\pi x\int_x^\infty I(y)(dy/y^2), \qquad (10)$$

which, for the case of an exponential absorption where $I(x)=I_0\exp(-x/L_a)$, becomes:

$$J_2(x)=2\pi I_0[\exp(-x/L_a) + (x/L_a)E_i(-x/L_a)]. \qquad (11)$$

Since for $x\gg L_a$ the logarithmic slope of $J_2(x)$ coincides with $1/L_a$, we must take $L_a=138$ g cm^{-2} in order to represent the observations in the lower atmosphere with a function of the type given by Eq. (11). The function $J_2(x)$ calculated with this value of L_a is represented by the dotted line in Fig. 9. Even though the accuracy of the measurements at high altitudes leaves much to be desired, it is certain that the experimental curve near the top of the atmosphere falls off with increasing depth much less rapidly than the theoretical dotted curve. This clearly indicates that, as the primary radiation penetrates the atmosphere, many secondary particles are created (probably, for the most part, protons and neutrons of comparatively low energy), which are capable of producing nuclear disintegrations. In fact, it is possible that these secondary particles are projected upwards in sufficient number to contribute appreciably to the rate of occurrence of low energy nuclear events at the top of the atmosphere.

Other experimental facts confirm the picture that develops from the above considerations. If we assume that protons and neutrons are generated in approximately equal numbers and have approximately equal probabilities of producing nuclear disintegrations, the number of nuclear disintegrations produced by the two types of particles should be approximately the same as long as we consider particles of sufficiently high energies so that the collision loss of protons can be neglected as compared with the nuclear absorption. At lower energies, however, most protons will be stopped by ionization losses before they have a chance to undergo a nuclear collision and the majority of the nuclear reactions will be produced by neutrons. The transition occurs in the neighborhood of the energy which corresponds to a proton range equal to the mean free path for nuclear collisions. This energy is of the order of $5\cdot10^8$ ev. Thus, the fact that practically all stars appear to be produced by non-ionizing rays is in agreement with the view that they are mostly produced by nucleons of energy smaller than $5\cdot10^8$ ev.

The absorption thickness for low energy nuclear events ($L_a=138$ g cm^{-2}) seems to be somewhat greater than the absorption thickness for high energy nuclear events ($L_a=125$ g cm^{-2}). It is possible that 138 g cm^{-2} corresponds to the absorption thickness in air for neutrons with energies of the order of several times 10^8 ev. The results of the recent measurements with the Berkeley 184-inch cyclotron (H3; C5) may be mentioned in this connection. These measurements indicate that the absorption thickness for neutrons of about 10^8-ev energy depends critically on the geometry of the experiment. In oxygen, the absorption thickness is 35 g cm^{-2} for a "good geometry" absorption measurement, 100 g cm^{-2} for a "poor geometry" absorption measurement. The even larger value for the absorption thickness in air of the star-producing radiation is not in contradiction with the hypothesis that it consists of neutrons because the average energy of cosmic-ray neutrons may be different from that of neutrons from the Berkeley cyclotron and because in cosmic-ray experiments even less collimation exists than in the "poor geometry" Berkeley experiments.

In Table III we give a tentative estimate of the rate of occurrence of various nuclear events at sea level. The evaluation of the rate of occurrence of stars is based on the observations of

Perkins (P1) and of Lattes *et al.* (L2). According to Lattes, approximately 10 stars per day are produced in one cubic centimeter of the emulsion at 2800-meter altitude. According to Perkins, the rate of production is one star per centimeter cube-day at sea level. In the paper of Lattes it is specified that only stars with more than 4 prongs are taken into consideration. No criterion for the selection of stars is specified in the paper of Perkins. In both experiments, the Ilford Nuclear Research Emulsion was used. It is stated by Perkins that 7 out of 8 stars represent disintegrations of light nuclei (C, O, N). Since the density of light elements in the emulsion is near to one, the number of stars per cubic centimeter of the emulsion should not be very different from the number of stars per gram of air.

The evaluation of the rate of occurrence of slow proton tracks is based upon the observations of Perkins (P1) who found, at sea level, 0.3 track per centimeter square-day. In the emulsion used, protons with energies up to about 80 Mev leave a detectable track. It is likely, however, that no single proton track of energy larger than about 20 Mev has been counted. Thus the number of proton tracks per unit area and unit time should represent the flux of protons of energy below 20 Mev.

The data obtained by various authors on the rate of production of slow neutrons in the atmosphere are not very consistent. The estimate given in Table III is based on the recent measurements taken by Yuan and Ladenburg (Y2) at various altitudes in an airplane (see Section 14). One will notice that the estimated rate of production of neutrons appears somewhat low when compared with the rate of production of stars because one would expect many more than two neutrons to be produced for every star with 5 prongs or more. It is difficult to judge how much significance can be attached to this discrepancy on account of the very tentative character of our intensity estimates.

TABLE III. Tentative estimate of rates of occurrence of various nuclear events. It is assumed that the variation of these rates with depth obeys an exponential law $\exp(-x/L_a)$ with $L_a = 138$ g cm^{-2} for depths greater than 250 g cm^{-2}.

Event	Unit	Experimental information	Adopted sea level value
Production of stars (5 prongs or more)	g^{-1} sec.$^{-1}$ (in air)	Experiments by Perkins at sea level, by Lattes *et al.* at 2800 m	10^{-5}
Production of neutrons	g^{-1} sec.$^{-1}$ (in air)	Yuan's observations at various altitudes	$2 \cdot 10^{-5}$
Slow proton tracks ($E < 20$ Mev?)	cm^{-2} sec.$^{-1}$	Sea level measurements by Perkins	$3.5 \cdot 10^{-6}$

22. Analysis of the Hard and Soft Components

According to our definitions, the intensity of the hard component is determined by measuring the coincidence rate between two Geiger-Mueller counters separated by 167 g cm^{-2} of lead. At sea level almost all of these coincidences are produced by mesons which traverse the two counters and the lead between them. At great altitudes, however, a large fraction of the coincidences is produced by high energy protons or, in general, by high energy N-rays if we assume that the N-radiation contains ionizing particles different from protons. A large fraction of the N-rays will undergo nuclear interactions in traversing the lead shield so that in many instances the coincidence will be produced by the primary particle traversing the upper counter and one of the secondary particles from the nuclear interaction traversing the lower counter. It may happen, too, that the counters both above and below the lead are discharged by secondary particles produced in a nuclear interaction of a neutral N-ray or of a charged N-ray which traverses neither of the two counters.

At the top of the atmosphere no mesons are present and the coincidences are all produced by the primary cosmic rays. For lack of better information, we shall make the assumption that the number of coincidences produced by N-rays varies with depth as $\exp(-x/L_a)$ where $L_a = 125$ g cm^{-2}. This assumption is consistent with the experimental data on the altitude variation of high energy N-rays discussed in Section 20.

To obtain the vertical intensity of mesons in the hard component, we extrapolate to zero thickness the curve representing the vertical intensity of the hard component[2] (see Fig. 2) and subtract from this curve a curve starting at $x = 0$ with the same ordinate and decreasing as $\exp(-x/125)$. The result of such an analysis is shown in Fig. 16. One will note that according to

[2] The criterion for the extrapolation will be discussed in Section 23.

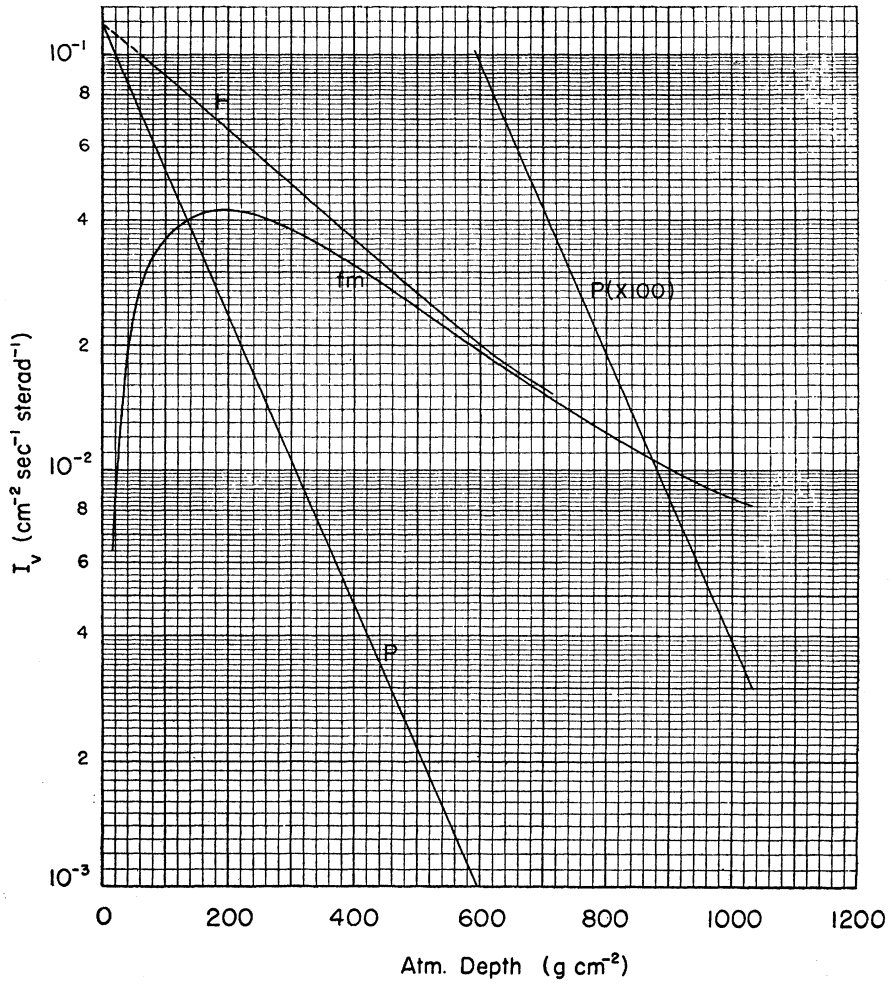

FIG. 16. Analysis of the hard component. The curve marked "*fm*" gives the vertical intensity of mesons with range greater than 167 g cm^{-2} of lead ("fast mesons"). The curve marked *P* represents the contribution of *N*-rays (high energy protons?) to the measured intensity of the hard component, but does not give an absolute value for the vertical intensity of these rays.

our assumptions, the contribution of protons (or more generally of *N*-rays) to the total intensity of the hard component at sea level amounts to 0.4 percent, a value consistent with the estimate of the number of high energy protons given in Table II.

The soft component, as measured with an absorber thickness of 5 g cm^{-2} of brass between the sensitive volumes of the counters, contains electrons of practically all energies above 10 Mev, mesons with momenta between $0.7 \cdot 10^8$ ev/c and $3 \cdot 10^8$ ev/c, protons with momenta between $4 \cdot 10^8$ ev/c and 10^9 ev/c. The intensities of mesons and protons in the soft component at atmospheric depths greater than 250 g cm^{-2} can be estimated, at least approximately, from the experimental data presented in Fig. 7 and Table II. The intensity of electrons can then be obtained by subtracting the meson and proton intensities from the intensity of the soft component given in Fig. 2. The results of this analysis are shown by the solid lines in Fig. 17. It appears that at all depths greater than 250 g cm^{-2} the proton and meson intensities represent a small fraction of the intensity of the soft component. Therefore, the large uncertainty which still exists in their precise values does not appreciably affect the evaluation of the electron intensity.

No accurate estimate of the electron intensity at depths smaller than 250 g cm^{-2} can be made at this time. The value of the intensity of the soft component in the upper layers of the atmosphere is uncertain, both because there is no good agreement between the various measurements of the

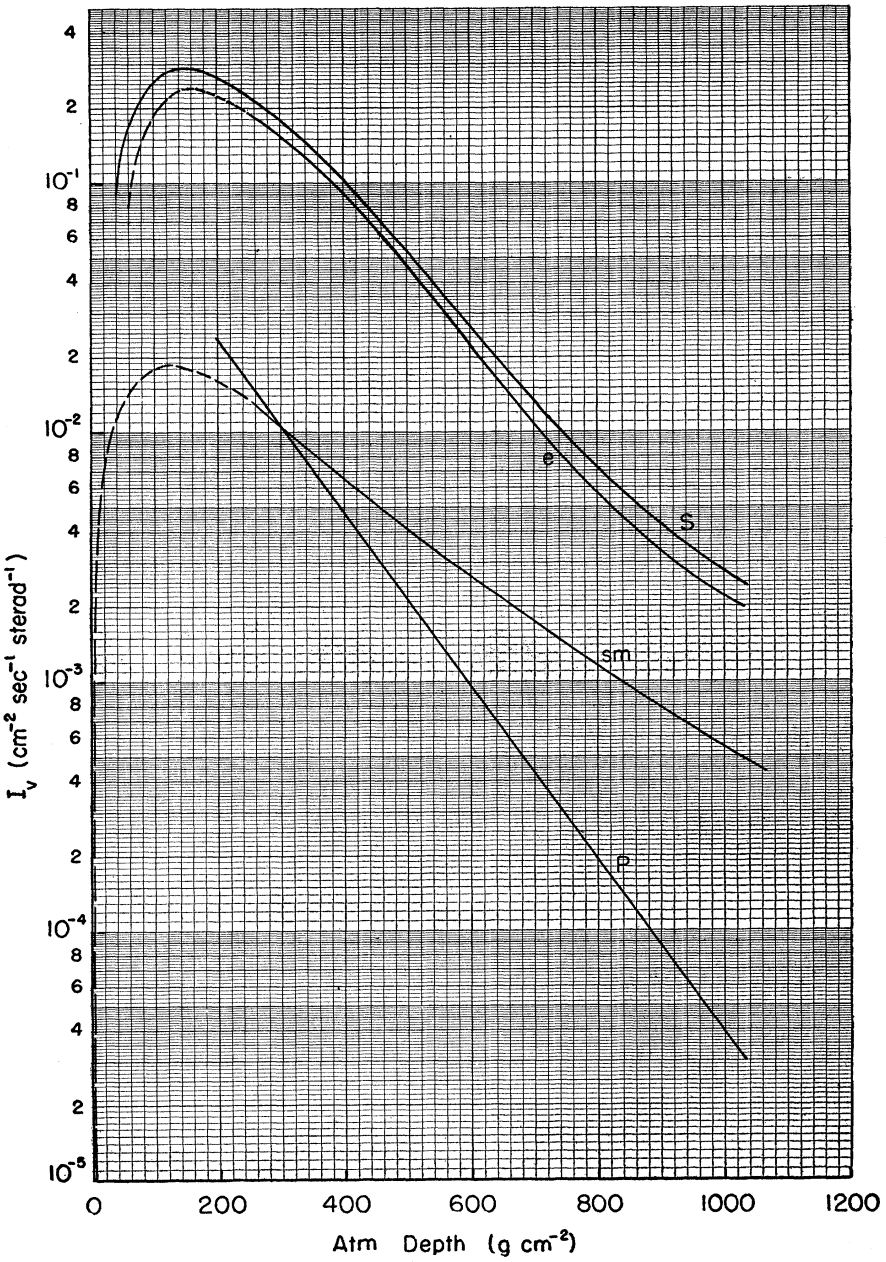

FIG. 17. Analysis of the soft component. The curves represent vertical intensities as a function of atmospheric depth for the following rays: "slow mesons," or practically all mesons with momenta smaller than $3 \cdot 10^8$ ev/c (*sm*); protons (or other charged *N*-rays) with momenta between $4 \cdot 10^8$ ev/c and 10^9 ev/c (*P*); electrons of practically all energies above 10^7 ev (*e*).

total intensity (see Fig. 2) and because the contribution of the hard component, which in this region consists largely of high energy primary particles, cannot be determined accurately. Moreover, no measurements exist of either the intensity of mesons or the intensity of protons in the soft component at depths less than 250 g cm^{-2}. While the meson intensity can be estimated with the help of some general arguments (see Section 23), no basis for an estimate of the proton intensity has been found.

In the discussion to be made below of the energy balance in cosmic rays, it is important to know, for each type of particle, the quantity

$$\int_0^{1030} I_v dx$$

TABLE IV. Track lengths in the atmosphere for the various components of cosmic rays.

Component	Track length (g cm^{-4} sec.$^{-1}$ sterad^{-1})
All ionizing particles $R>5$-g cm^{-2} brass	133±17
Mesons 5-g cm^{-2} brass $<R<100$-g cm^{-2} air	6±3
Mesons $R>100$-g cm^{-2} air	24±2
Protons 5-g cm^{-2} brass $<R<100$ g cm^{-2} air	6±3
Ionizing N-rays (Protons?) $R>100$-g cm^{-2} air	8±4
Electrons (by difference) $R>5$-g cm^{-2} brass	89±18

which may be described as the *track length* in the atmosphere. An evaluation of the track lengths for the various components of cosmic rays is given in Table IV. The errors indicated represent an estimate of the various experimental uncertainties. In the evaluation of the track length of ionizing N-rays with $R>100$ g cm^{-2}, allowance has been made for the fact that the detection efficiency of a cosmic-ray telescope for these particles is likely to be greater than for mesons (see Section 19).

23. The Energy of the Meson Component

In order to describe the energy exchanges which take place in the atmosphere, we shall define, for any given group of cosmic-ray particles, a function $k(x)$ such that $k(x)d\omega$ represents the energy which is lost per unit time in one gram of air at the depth x by particles of the given group arriving within the solid angle $d\omega$ in the vertical direction. The quantity $k(x)$ will be measured in ev g^{-1} sec.$^{-1}$ sterad^{-1}.

The meson component in air loses energy by collision processes and by decay (the energy loss by radiation can be neglected for meson energies smaller than about 10^{12} ev). We shall consider separately the mesons of the hard and of the soft components, which, for brevity, will be denoted as "fast mesons" and "slow mesons," respectively.

For fast mesons in air the rate of dissipation of energy by collision may be considered as independent of energy and equal to $2\cdot10^6$ ev g^{-1} cm^2. Therefore, the collision loss of the fast meson component is represented by the expression

$$k_c^{(fm)}(x)=2\cdot10^6 I_v^{(fm)}(x) \quad \text{ev g}^{-1}\text{ sec.}^{-1}\text{ sterad}^{-1}, \quad (12)$$

where $I_v^{(fm)}$ is the vertical intensity of fast mesons.

If we consider a group of mesons with energies large compared with their rest energy, the total energy released by the mesons which decay in a layer of air of one g cm^{-2} is independent of the energy distribution of the mesons and is equal to $\mu c/\tau\rho$ times the number of incident mesons where ρ is the density of air (R6). Therefore, the decay loss of the fast meson component is represented by the expression:

$$k_d^{(fm)}(x)=(\mu c/\tau\rho)I_v^{(fm)}(x). \quad (13)$$

To find the expressions for the collision loss and the decay loss of slow mesons, we assume that at all altitudes the differential range spectrum of mesons is flat between 0 and 100 g cm^{-2}. As mentioned in Section 6, this seems to be approximately true at all altitudes at which measurements were taken. The average energy loss by collision of slow mesons is then given by the maximum kinetic energy of the slow meson group ($E_m=2.2\cdot10^8$ ev) divided by the corresponding range ($R_m=100$ g cm^{-2}). We obtain thus

$$k_c^{(sm)}(x)=2.2\cdot10^6 I_v^{(sm)}(x) \quad \text{ev g}^{-1}\text{ sec}^{-1}\text{ sterad}^{-1}, \quad (14)$$

where $I_v^{(sm)}$ is the vertical intensity of slow mesons.

Under the same assumption of a uniform distribution in range, the decay loss of slow mesons can be shown to have the following value

$$k_d^{(sm)}(x)=1.2(\mu c/\tau\rho)I_v^{(sm)}(x). \quad (15)$$

Last, one has to consider the mesons which are brought to rest in air and subsequently disintegrate or disappear by nuclear absorption. The energy which is subtracted from the meson beam through this process is given by the expression

$$k^{(mr)}(x)=(I_v^{(sm)}/R_m)\mu c^2, \quad (16)$$

where $I_v^{(sm)}/R_m$ represents the differential intensity of slow mesons.

The values of the various energy losses of mesons, computed by means of Eqs. (13), (15), and (16), and of the measured values of $I_v^{(fm)}$ and $I_v^{(sm)}$, are plotted as solid lines in Fig. 18. In order to extrapolate the curves to the smaller depths, let us investigate the behavior of the decay loss at the limit for $x=0$. We consider for this purpose mesons of a given momentum p and denote with $K(x)$ the energy per gram second steradian which goes into the production of these mesons at the depth x. If x is sufficiently small, collision losses can be neglected, and we can

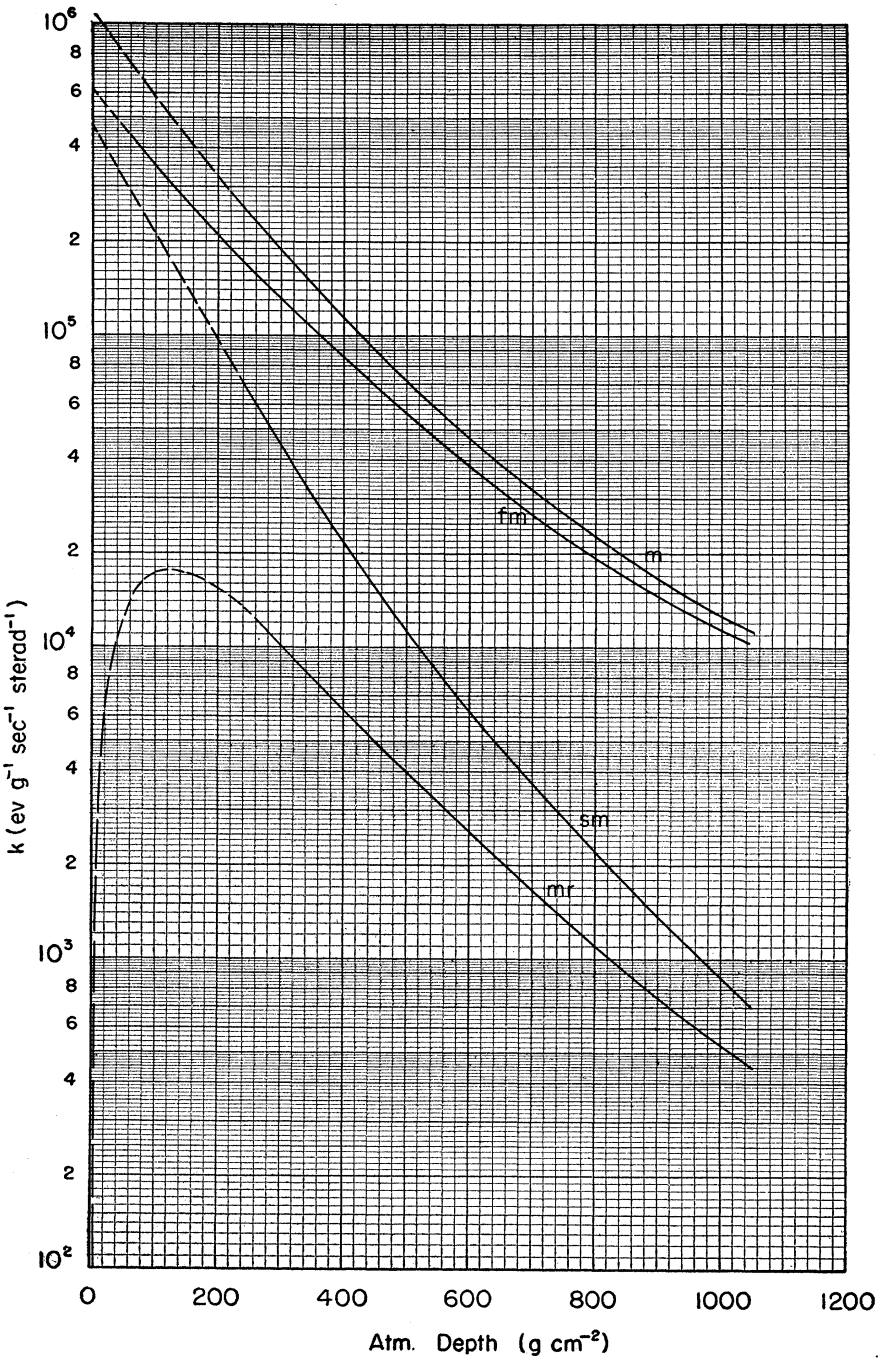

FIG. 18. The decay loss in the atmosphere of the various meson components, namely, fast mesons (*fm*), slow mesons (*sm*), and mesons at rest (*mr*). The curve marked *mr* includes the rest energy of mesons which undergo nuclear capture in addition to the energy of those which undergo spontaneous decay. The curve marked *m* is the sum of the other three curves.

assume also that the ratio $x/\rho = z_0$, where z_0 is a constant (see Fig. 21). Then the probability that a meson produced at the depth x will disintegrate in the depth interval dx_1 at x_1 is given by

$$(z_0/\lambda)(x/x_1)^{z_0/\lambda}(dx_1/x_1),$$

where $\lambda = \tau p/\mu$ represents the mean free path before decay. Therefore the decay loss k_d of the meson beam at the depth x_1 has the following expression

$$k_d(x_1) = (z_0/\lambda)x_1^{-(z_0/\lambda)-1}\int_0^{x_1} K(x)x^{z_0/\lambda}dx.$$

If we develop $K(x)$ in a Taylor series near $x=0$ and integrate, we obtain for $k_d(x_1)$ the series

$$k_d(x_1) = [K(0)/(1+\lambda/z_0)] + [K'(0)/(1+2\lambda/z_0)]x_1 + \cdots. \quad (17)$$

At the top of the atmosphere, therefore, the following relations hold:

$$k_d(0) = K(0)/(1+\lambda/z_0),$$
$$\left(\frac{d\ln k_d}{dx}\right)_{x=0} = \frac{1+(\lambda/z_0)}{1+(2\lambda/z_0)}\left(\frac{d\ln K}{dx}\right)_{x=0}. \quad (18)$$

One sees that at very small atmospheric depths the amount of energy lost by the meson beam in one gram of air is always smaller than the amount of energy which goes into the meson beam in the same mass of air.[3] The values of λ for mesons of the "slow" group are between 0 and $2\cdot10^5$ cm. On the other hand, near the top of the atmosphere $z_0 = 6.4\cdot10^5$ cm. For slow mesons, therefore, the average value of the fraction $(1+\lambda/z_0)/(1+2\lambda/z_0)$ is between 1 and 0.8 and one can assume, for a first approximation, that the logarithmic derivative of $k_d(x)$ near the top of the atmosphere is equal to the logarithmic derivative of $K(x)$. According to our assumption, mesons are produced by high energy N-rays which vary with depth as $\exp(-x/125)$. We therefore conclude that $d(\ln k_d^{(sm)})/dx$ approaches $1/125$ as x approaches zero. On the other hand, Fig. 18 shows that $d(\ln k_d^{(sm)})/dx$ is approximately equal to $1/125$ already at $x = 250$ g cm^{-2}. It is thus natural to assume that $k_d^{(sm)}$ is represented by the function $\exp(-x/125)$ between 0 and 250 g cm^{-2}, as shown by the broken line in Fig. 18.

For the fast meson group, the direct determination of k_d extends to considerably greater heights than for the slow meson group. Since our considerations show that one should not expect any sudden change in slope of k_d in the neighborhood of $x=0$, a linear extrapolation to $x=0$ of the experimental curve giving $\ln k_d^{(fm)}$ as a function of x appears justified. From the extrapolated values of $k_d^{(fm)}$ and $k_d^{(sm)}$ one can then compute, by means of Eqs. (13) and (15), the corresponding values for $I_v^{(fm)}$ and $I_v^{(sm)}$. These are shown in Figs. 16 and 17.

Integration with respect to x of the functions representing the various energy losses per gram second steradian yields the corresponding energy losses (per second steradian) of the meson beam in a vertical column of 1 cm^2 cross section. The results are shown in Table V. The collision losses underground ($x > 1030$ g cm^{-2}) were computed from the experimental data on the meson spectrum at sea level. For the total energy loss of mesons one obtains

$$W^{(m)} = 289\cdot10^6 \text{ ev cm}^{-2} \text{ sec.}^{-1} \text{ sterad}^{-1}. \quad (19)$$

This quantity represents also the total energy (per second steradian in the vertical direction) of the mesons produced in a vertical column of one cm^2 cross section extending from the top of the atmosphere to the maximum depth at which meson production occurs.

24. Analysis of the Electron Component

Some of the electrons observed in the atmosphere arise from collision processes of mesons and from the subsequent multiplication of the electrons thus produced. Since the meson intensity varies slowly with depth and since collision processes give rise to electrons of small average energy, one can compute the number of electrons of this origin under the assumption that the meson intensity does not vary appreci-

[3] This shows the fallacy of the following apparently obvious argument: "Near the top of the atmosphere, the density of air is so small that mesons disintegrate before they traverse any appreciable thickness of the atmosphere; *therefore* the energy which goes into mesons in a given layer of atmosphere equals the energy which the mesons lose in the same layer."

ably over a distance equal to the average range of the showers produced by the collision electrons. As already mentioned, the minimum energy of the electrons in the soft component is about 10^7 ev. The number of electrons of energy larger than this value arising from collision processes of mesons can be obtained from the calculation of Rossi and Klapman (R7) and of Tamm and Belenky (T1). At sea level it is 6.7 percent of the number of fast mesons. Slow mesons do not give any contribution since the maximum energy which a $3\cdot10^8$ ev/c meson can transfer to an electron is 9 Mev. In the analysis of the electron component, we shall assume that the ratio of collision electrons to fast mesons is the same at all altitudes, even though in fact, this ratio depends somewhat on the meson spectrum which changes with altitude. The error thus made will not affect appreciably the evaluation of the intensity of electrons from other sources because the relative contribution of collision electrons to the total electron intensity decreases rapidly with increasing altitude. In addition, we will neglect the electrons produced by collision processes of protons, for which the maximum transferable energy is about 100 times smaller than for mesons of equal momentum.

According to our assumptions, there are two other major sources of electronic radiation beside the collision processes: namely meson decay and nuclear interactions. It is safe to assume that the average energy of the electrons or photons produced in these phenomena is large compared to the critical energy in air. It can then be shown (see R7; T1) that the actual energy distribution of these electrons or photons has very little influence on the energy distribution of the low energy electrons arising from their multiplication. Therefore, from the number of electrons with energy larger than a given value incident upon one square centimeter, it is possible to calculate the energy dissipated in one gram of air by electrons of *all* energies. If we consider electrons incident in the vertical direction and use the results of Rossi and Klapman, we obtain the following relation:

$$k^{(e)}=3.26\cdot10^6 I_v^{(e)} \text{ ev g}^{-1} \text{ sec.}^{-1} \text{ sterad}^{-1}, \quad (20)$$

where $I_v^{(e)}$ is the vertical intensity of electrons of energy larger than 10^7 ev and $k^{(e)}$ is the energy loss per gram second steradian of electrons of all energies arising from decay of mesons and nuclear interactions. The quantity $k^{(e)}(x)$ is plotted as a function of atmospheric depth x in Fig. 19. The values corresponding to depths smaller than 250 g cm^{-2}, plotted with a broken line, are very uncertain as are the corresponding values of $I_v^{(e)}$ (see Section 22).

TABLE V. Energy losses of mesons, in Mev cm^{-2} sec.$^{-1}$ sterad^{-1}.

Depth interval (g cm^{-2})	$0<x<250$	$250<x<1030$	$x>1030$	Total
Collision loss				
Fast mesons	17	31	37	85
Slow mesons	8	6	—	14
Decay loss				
Fast mesons	84	38	—	122
Slow mesons	52	9	—	61
Mesons at rest	4	3	—	7
Total energy loss	165	87	37	289

The total energy loss of the electronic component in the atmosphere can be computed by integrating the curve in Fig. 19. One obtains

$$W^{(e)}=285\cdot10^6 \text{ ev cm}^{-2} \text{ sec.}^{-1} \text{ sterad}^{-1}. \quad (21)$$

Since the energy of the electronic component at sea level is negligible as compared with $W^{(e)}$, this quantity represents the total energy (per second steradian in the vertical direction) which goes into electronic radiation in a vertical column of atmosphere of 1 cm^{-2} cross section.

The fraction of the energy released by the decay of mesons which goes into the electronic component is not yet known with certainty.[4] It is thus not possible to determine unambiguously the relative contribution of decay processes ($k_d^{(e)}$) and nuclear interactions ($k_n^{(e)}$) to the total electron loss ($k^{(e)}$). The quantity $k_d^{(e)}$ has been computed theoretically in the lower part of the atmosphere, for the case that the above fraction is one, by the method described by Rossi and Greisen (R6). Namely, the energy dissipated by electrons in one gram of air at a certain depth x has been put equal to the energy which goes into the electronic component in one gram of air at a depth $x-\bar{x}$ where $\bar{x}$ is the average range of the showers initiated by the electrons or photons arising from the decay.

[4] It may be noted that this fraction has the same value in the laboratory system as in the frame of reference in which the meson is at rest.

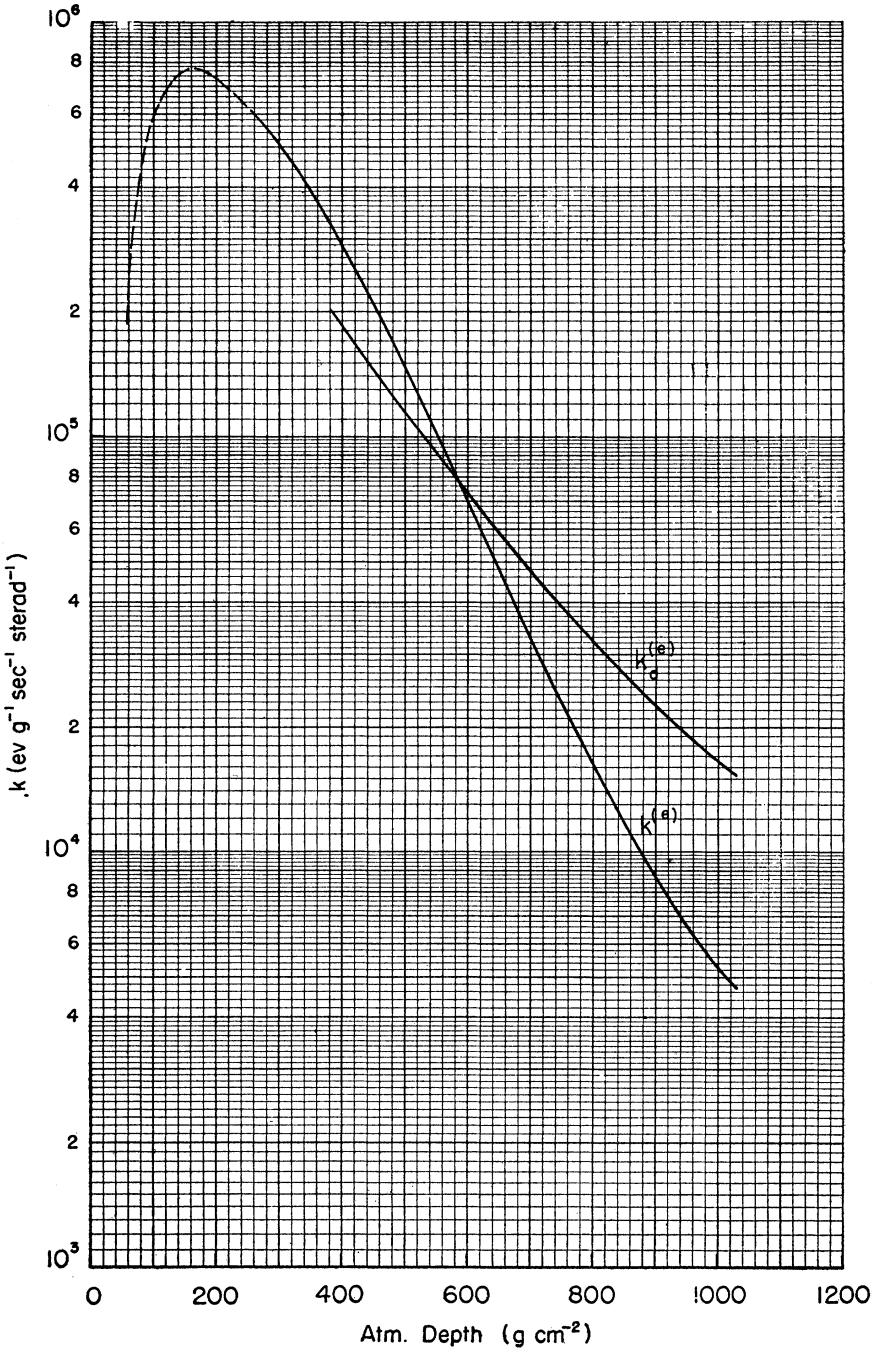

FIG. 19. The curve marked $k^{(e)}$ gives the energy loss in the atmosphere of cosmic-ray electrons (exclusive of collision electrons). The curve marked $k_d^{(e)}$ gives the energy loss of electrons arising from the decay of mesons, computed under the assumption that the whole energy set free by the decay goes into the electronic component.

The average range $\bar{x}$ was taken as equal to 130 g cm^{-2} for the decay products of fast mesons, to 65 g cm^{-2} for the decay products of slow mesons, to zero for the decay products of mesons at rest. The results of the calculation are shown by the curve marked $k_d^{(e)}$ in Fig. 19. This curve, as pointed out repeatedly (B1; R6; B3), rises with decreasing depth much less rapidly than the observed electron intensity, which shows that the majority of the electrons observed at high elevation do not originate from the decay of mesons. At sea level, the absolute value of

$k_d^{(e)}$ is more than twice that of $k^{(e)}$. If taken at face value, this result would indicate that *less than one-half* of the decay energy of mesons goes into electronic radiation. This conclusion may not be considered as final because of the many uncertainties that still exist in the evaluation of the experimental data, even though a reasonable estimate of these uncertainties gives a possible error of 20 percent for the ratio $k_d^{(e)}/k^{(e)}$, while $k_d^{(e)}/2$ exceeds $k^{(e)}$ by about 40 percent. In any case, the possibility that the whole decay energy goes into electronic radiation is surely ruled out.

From Table V it appears that the total energy of the decay products of mesons is $190 \cdot 10^6$ ev cm^{-2} sec.$^{-1}$ sterad^{-1}. Since not more than one-half of this energy goes into electronic radiation, and since the total energy W^e of the electronic radiation is $285 \cdot 10^6$ ev cm^{-2} sec.$^{-1}$ sterad^{-1}, the minimum amount of energy in the electronic radiation to be accounted for by nuclear processes is

$$W_n^{(e)} = 190 \cdot 10^6 \text{ ev cm}^{-2} \text{ sec.}^{-1}.$$

It is interesting to compare this value with the total energy $W^{(m)}$ of the meson component, which in Section 23 was found to be $289 \cdot 10^6$ ev cm^{-2} sec.$^{-1}$ sterad^{-1}. It appears that $W_n^{(e)}$ and $W^{(m)}$ are of the same order of magnitude, but their exact ratio cannot be determined at this time. If we take into account the uncertainty in the value of the total electron energy and the uncertainty in the fraction of this energy which is accounted for by meson decay we conclude that the value of $W_n^{(e)}$ could be as low as $W^{(m)}/2$ or as high as $W^{(m)}$.

25. The Total Energy of Cosmic Rays at Latitudes Greater than 45°

The total amount of energy coming into the earth in the form of cosmic rays per square centimeter second steradian can be estimated by adding up the amounts of energy dissipated in the various secondary processes initiated by these rays.

The result of such an estimate is given in Table VI.[5] The energy dissipated by collision processes, in the atmosphere and underground, by ionizing particles with ranges larger than 5 g cm^{-2} of brass was computed from the data presented in the previous sections. The average collision loss of ionizing N-rays (protons?) with $R > 100$ g cm^{-2} of air was taken as equal to 2 Mev per g cm^{-2}. The average collision loss of protons with R between 5 g cm^{-2} of brass and 100 g cm^{-2} of air was arbitrarily taken as equal to $6 \cdot 10^6$ ev per g cm^{-2}. (It would be equal to $4 \cdot 10^6$ if these protons were uniformly distributed in range; actually their differential range spectrum increases with decreasing R.) The energy (per centimeter square second steradian) of the primary radiation, incident vertically, which goes in the production of the particles considered above, is not exactly equal to the energy dissipation by these particles because in the secondary processes in which secondary particles are created direction is not preserved. The estimated difference between the two energies is of the order of 10 percent (see Appendix, Section 30).

TABLE VI. Estimate of the total energy of cosmic rays.

Collision loss of all mesons in the atmosphere	62-Mev cm^{-2} sec.$^{-1}$ sterad^{-1}
Collision loss of all mesons underground	37-Mev cm^{-2} sec.$^{-1}$ sterad^{-1}
Collision loss of ionizing N-rays (protons?), $R > 100$-g cm^{-2} air	16-Mev cm^{-2} sec.$^{-1}$ sterad^{-1}
Collision loss of protons 5-g cm^{-2} brass $< R <$ 100-g cm^{-2} air	36-Mev cm^{-2} sec.$^{-1}$ sterad^{-1}
Collision loss of electrons (exclusive of collision electrons)	285-Mev cm^{-2} sec.$^{-1}$ sterad^{-1}
Sum of the above collision losses	436-Mev cm^{-2} sec.$^{-1}$ sterad^{-1}
Corrected for angular spread	480-Mev cm^{-2} sec.$^{-1}$ sterad^{-1}
Energy loss by nuclear disintegrations	120-Mev cm^{-2} sec.$^{-1}$ sterad^{-1}
Neutrino loss	95-Mev cm^{-2} sec.$^{-1}$ sterad^{-1}
Total incident energy	695-Mev cm^{-2} sec.$^{-1}$ sterad^{-1}

The item listed as "energy loss by nuclear disintegrations" includes the energy spent in disrupting nuclei as well as the energy dissipated by neutrons, protons or other nuclear fragments which are produced in these disintegrations and are not detected by a cosmic-ray telescope. No accurate determination of the energy loss by nuclear disintegrations can be made at this time. On account of the discrepancy between the experimental data on stars and on neutrons (see Table III), any estimate of the rate of occurrence of nuclear disintegrations at sea level is uncertain by at least a factor two. The value chosen here is $2 \cdot 10^{-5}$ g^{-1} sec.$^{-1}$ in air. From the curve in Fig. 9 one then obtains a value of 3.6 cm^{-2} sec.$^{-1}$ for the total number of nuclear disintegrations in the

[5] A similar estimate of the total cosmic-ray energy was reported by H. A. Bethe at the Shelter Island Conference in June 1947. The results of Bethe's estimate are in fair agreement with those presented here.

atmosphere. The average energy which is released in a nuclear disintegration and is not spent in the production of rays detected by a cosmic-ray telescope is also difficult to determine. We shall assume that this energy is equal to 10^8 ev and we thus obtain for the total energy release in the atmosphere the value of $3.6\cdot10^8$ ev cm^{-2} sec.$^{-1}$. The fraction of this energy which arises from primary rays incident within one steradian is $3.6\cdot10^8/\pi=1.2\cdot10^8$ ev cm^{-2} sec.$^{-1}$ sterad^{-1}. Last, we have to consider the energy which disappears in the production of "neutrinos" or other undetectable neutral particles. We have taken this energy as equal to one-half of the total decay loss of mesons, or 95-Mev g cm^{-2} sec^{-1} sterad^{-1}. This is a minimum estimate because it is possible that less than half of the decay energy goes into electronic radiation or that undetectable rays are produced in processes other than the disintegration of mesons.

The error in the determination of the total collision loss is estimated to amount to $60\cdot10^6$ ev cm^{-2} sec.$^{-1}$ sterad^{-1}, and it arises mainly from the uncertainty in the value for the track length of all ionizing particles (see Table IV). The uncertainty in the energy loss by nuclear disintegrations amounts to about $100\cdot10^6$ ev cm^{-2} sec.$^{-1}$ sterad^{-1} and the uncertainty in the "neutrino" loss by the decay of mesons amounts to about $50\cdot10^6$ ev cm^{-2} sec.$^{-1}$ sterad^{-1}. Thus if the decay of mesons is the only process in which undetectable rays are produced, the total energy of the primary cosmic radiation at geomagnetic latitudes greater than 45° has the value

$$W^{(p)}=(695\pm130)\cdot10^6 \text{ ev cm}^{-2}\text{ sec.}^{-1}\text{ sterad}^{-1}. \quad (22)$$

The number of primary cosmic rays can be obtained by dividing the total incoming energy by the average energy of the primary particles. From the geomagnetic effects, it is known that the minimum energy of the primary particles, if protons, is about $4\cdot10^9$ ev. From the same effects the average energy has been estimated to be approximately 10^{10} ev. If we adopt this figure we conclude that the directional intensity of the primary particles is

$$I^{(p)}=(0.07\pm0.013) \text{ cm}^{-2}\text{ sec.}^{-1}\text{ sterad}^{-1}. \quad (23)$$

This number may be compared with the value of 0.12 cm^{-2} sec.$^{-1}$ sterad^{-1} for the "intensity of the hard component" at the top of the atmosphere shown in Fig. 2. It may be compared, too, with the total intensity at the top of the atmosphere which has been measured recently by Van Allen and Tatel (V4) with a Geiger-Mueller counter placed in the nose of a rocket at a large distance from the main body of the rocket, and for which again a value of 0.12 cm^{-2} sec.$^{-1}$ sterad^{-1} has been obtained. For the reasons discussed previously (see Section 19), both of these values are probably greater than the actual intensity of the primary radiation (except that a latitude effect may have to be taken into account for the second measurement, which was carried out at 40° latitude). Thus the difference between the values of the primary intensity obtained from direct measurements at high altitude and from the evaluation of the total cosmic-ray energy does not prove that the amount of energy which goes into neutrinos or other undetectable rays is much greater than one-half the decay energy of mesons.

APPENDIX

26. The Standard Atmosphere

The relations between atmospheric depth, altitude above sea level, and density of air in atmosphere as given by the Report No. 538 of the National Advisory Committee for Aeronautics are shown in Figs. 20 and 21.

27. Momentum and Energy Loss of Heavy Particles

Energy range relations and momentum range relations for ionizing particles in various substances are shown in Figs. 22 and 23. They were obtained from the calculations of Wick (W2) and of Smith (S10), and are valid for all particles for which energy losses by radiation and by nuclear interactions are negligible compared with the energy loss by collision. Figure 24 gives dR/dE and dR/dp in air as functions of R.

28. Angular Divergence in the Production of Secondary Particles by Nuclear Collisions

Let us consider an inelastic collision between a nucleon of momentum p and a nucleon at

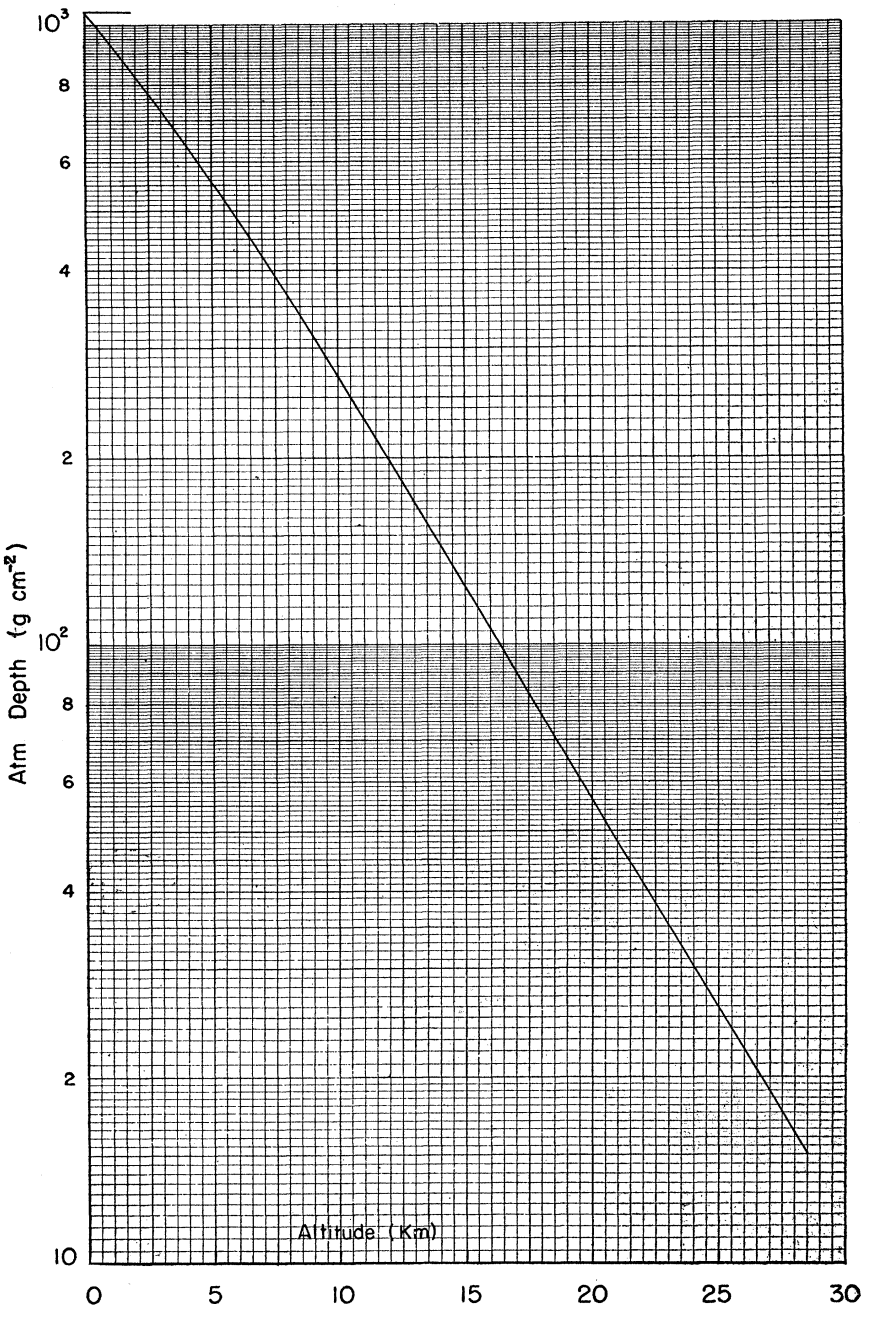

FIG. 20. Atmospheric depth as a function of altitude in the standard atmosphere.

rest in which two mesons are created. The equation

$$\beta_c/(1-\beta_c^2)=p/2Mc \qquad \text{(A1)}$$

determines the velocity $c\beta_c$ of the two nucleons in the frame of reference in which their center of mass is at rest. Suppose that after the collision, in the center of mass system, the two nucleons are left each with a total energy equal to α times their rest energy, while the remaining energy is split equally between the two mesons. The total energy E_0, momentum p_0, and velocity β_0 of *each*

particle in the center of mass system after the collision are given by the following equations:

Nucleons:

$$E_0=\alpha Mc^2, \quad p_0=\beta_0 E_0/c, \quad 1/(1-\beta_0^2)^{\frac{1}{2}}=\alpha.$$

Mesons:

$$E_0=Mc^2[(1/(1-\beta_c^2)^{\frac{1}{2}})-\alpha], \quad p_0=\beta_0 E_0/c,$$
$$1/(1-\beta_0^2)^{\frac{1}{2}}=(M/\mu)[(1/(1-\beta_c^2)^{\frac{1}{2}})-\alpha]. \quad \text{(A2)}$$

Suppose further that in the center of mass system the nucleons and the mesons are ejected at right angles to the initial line of motion of the nucleons. Then the energies E and the angles of emission ψ of each particle in the laboratory system are given by the following equations:

Nucleons:

$$E=\alpha Mc^2/(1-\beta_c^2)^{\frac{1}{2}}, \quad \tan\psi=(\beta_0/\beta_c)(1-\beta_c^2)^{\frac{1}{2}}.$$

Mesons:

$$E=Mc^2[(1/1-\beta_c^2)-(\alpha/(1-\beta_c^2)^{\frac{1}{2}})],$$
$$\tan\psi=(\beta_0/\beta_c)(1-\beta_c^2)^{\frac{1}{2}}. \quad \text{(A3)}$$

The various functions of β which appear in Eqs. (A1), (A2), and (A3) are represented graphically in Fig. 25. As examples, some E's and ψ's corresponding to $p/Mc=10$ are listed in Table VII.

29. Estimate of the Cosmic-Ray Energy Projected Upwards in Nuclear Interactions

Let us assume that the primary particles are protons. In the collisions between these protons and atomic nuclei mesons and electrons or photons are produced (either directly or indirectly). Mesons of momentum p projected upwards decay after an average path given by $p\tau/\mu$. The average angle through which they are deflected by the earth's magnetic field H before decay is given by the average path divided by radius of curvature R. If the trajectory of the particles is perpendicular to the field, $R=pc/300H$ and the deflection angle is equal to $300H\tau/\mu c$. Since H is of the order of $\frac{1}{2}$-gauss, this angle is of the order of 0.1. For a first approximation we may neglect this deflection and assume, *for the purpose of the conservation of momentum*, that the meson decays immediately after being produced. We shall now assume that

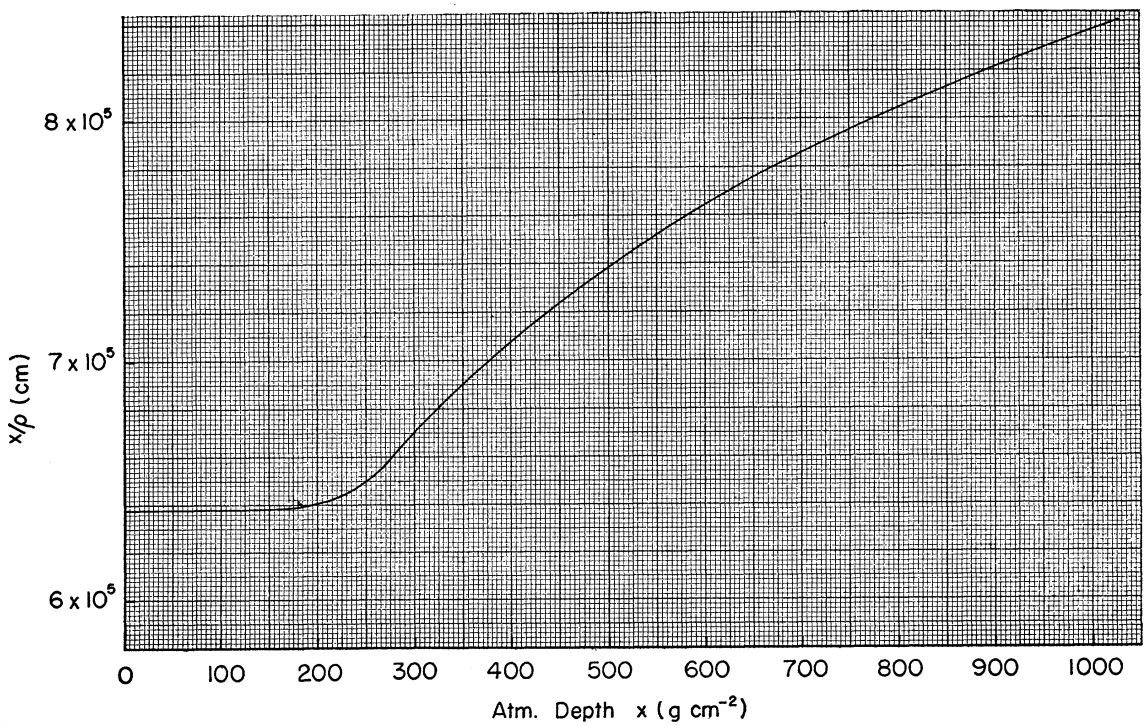

FIG. 21. x/ρ as a function of x in the standard atmosphere; x is the atmospheric depth, ρ the density of air.

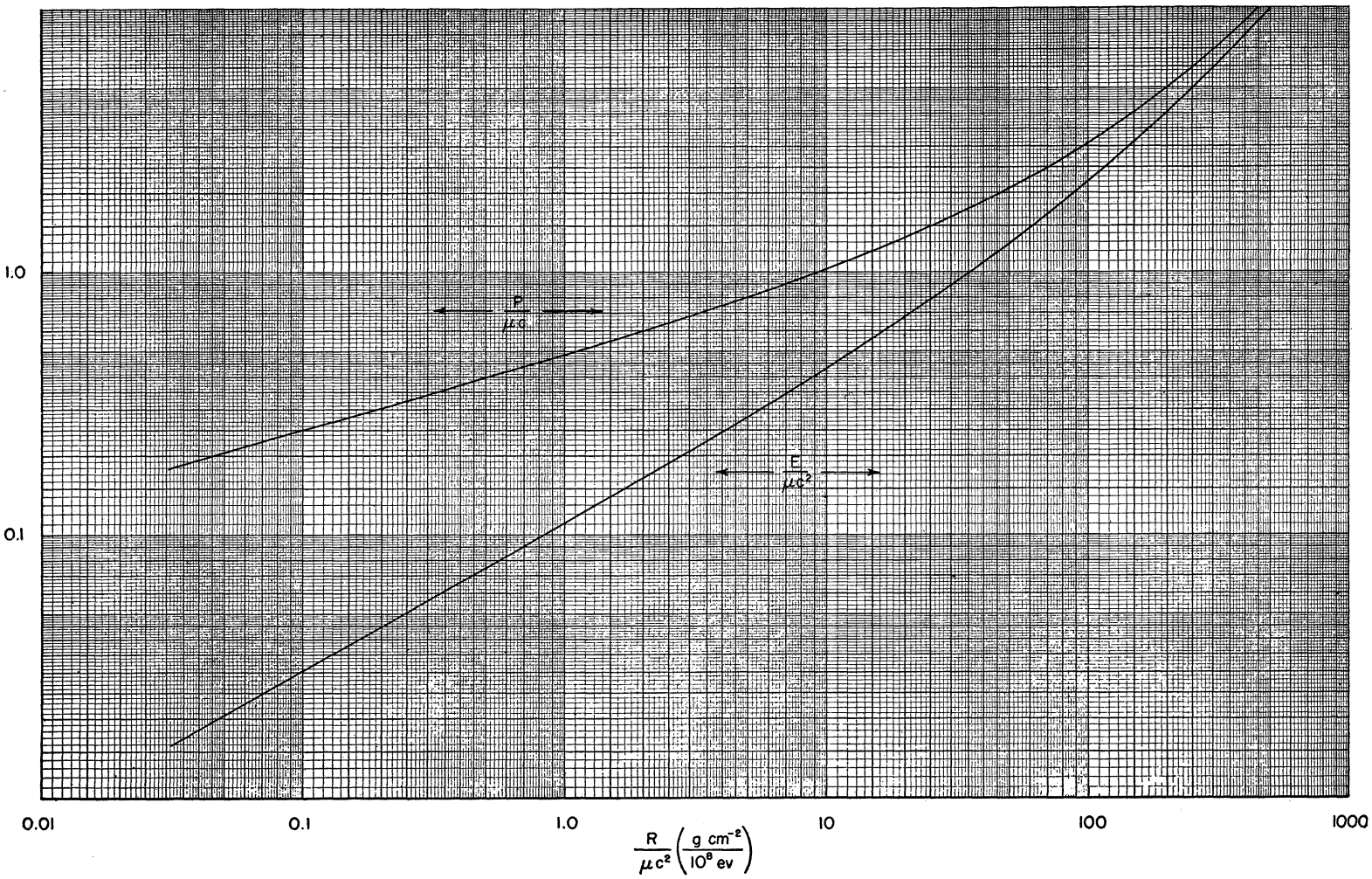

FIG. 22. $p/\mu c$ and $E/\mu c^2$ as functions of $R/\mu c^2$ in air; p is the momentum, E the kinetic energy, R the range, μ the mass. The curves are valid for particles of any mass, provided that energy losses by radiation and nuclear interactions are negligible compared with collision losses (after Smith, S10).

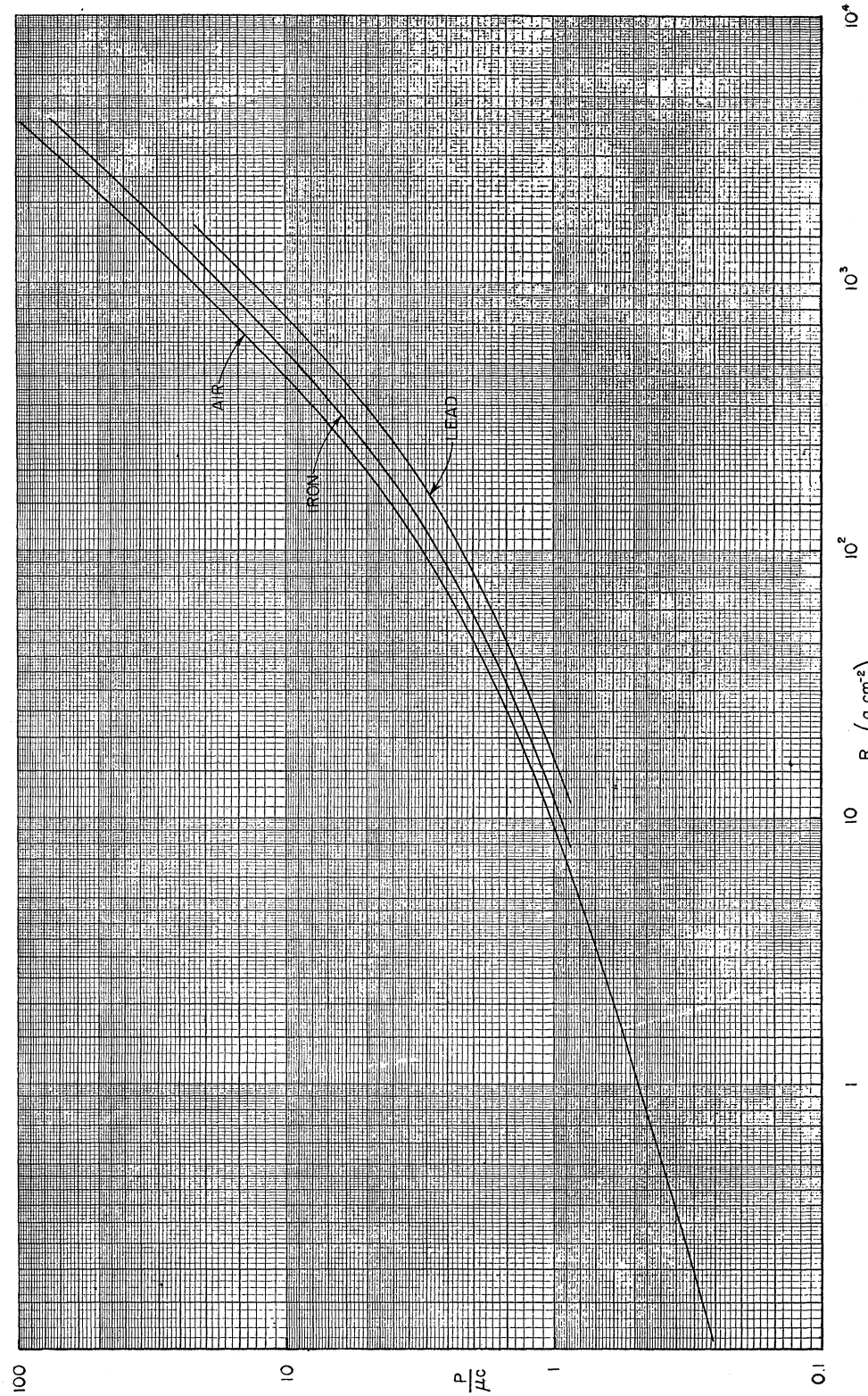

FIG. 23. $p/\mu c$ as a function of $R/\mu c^2$ in air, iron, and lead; p is the momentum, R the range, μ the mass. The curves are valid for particles of any mass provided that energy losses by radiation and by nuclear interactions are negligible compared with collision losses (after Wick, W2).

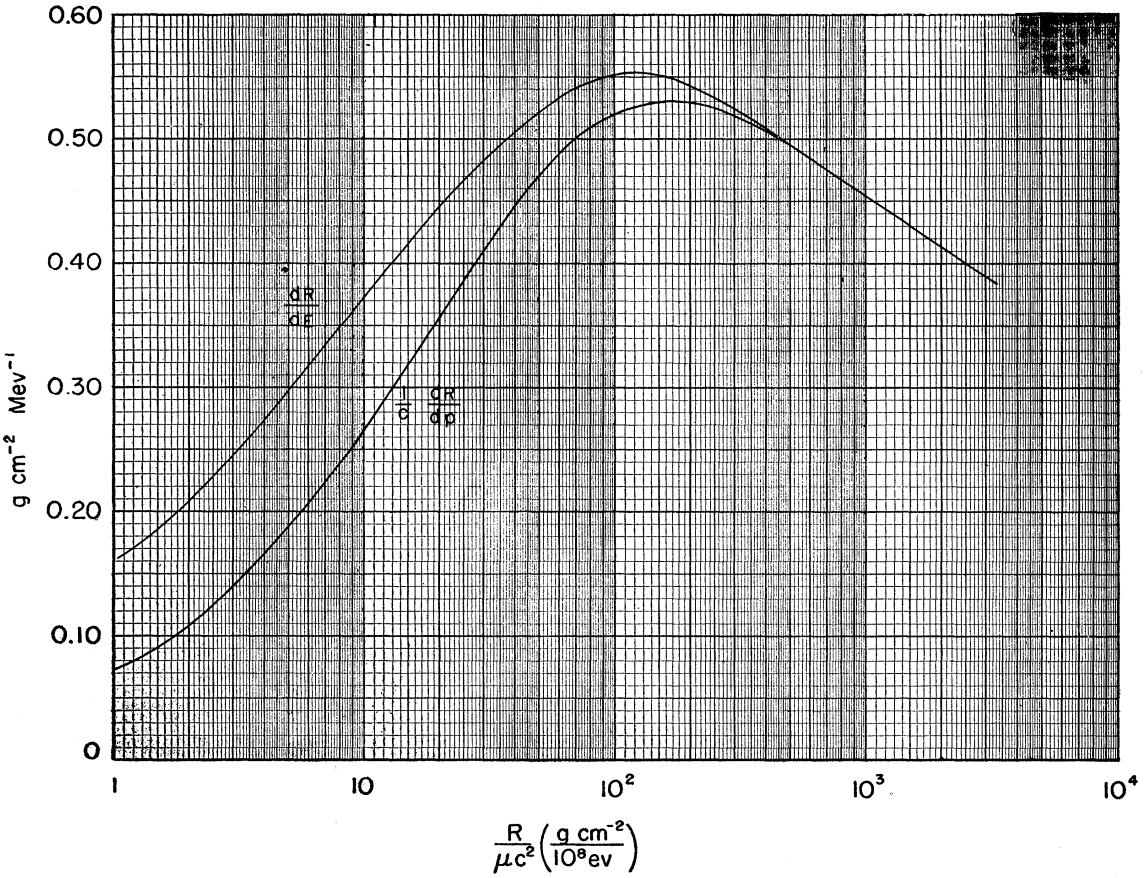

FIG. 24. dr/dE and dR/dp as functions of $R/\mu c^2$. R is the range in air, E is the energy, p is the momentum.

the inelastic collisions in which secondary particles are produced can be regarded as collisions between two free nucleons, and shall consider the phenomenon in the frame of reference in which the center of mass of the two nucleons is at rest. In this frame of reference, let E_0 be the total average energy of the secondary light particles (electrons, photons, neutrinos) regardless of whether they are created directly or as a consequence of a later disintegration process. Nothing is known *a priori* about the angular distribution of these particles, except that it must be, on the average, symmetric with respect to a plane through the center of mass and perpendicular to initial line of flight of the nucleons. We consider, therefore, two extreme cases in which (a) the secondary light particles are emitted in the two opposite directions parallel to the line of flight and (b) the secondary light particles are emitted at right angles to the line of flight. The secondary light particles are assumed to have relativistic velocities. In case (a) the total average momentum of the particles traveling in each of the two opposite directions is $E_0/2c$. If we transform back to the laboratory system we obtain the following values for the total average energies of the two groups of particles:

in the forward direction:

$$(E_0/2)[(1+\beta_c)/(1-\beta_c^2)^{\frac{1}{2}}],$$

in the backward direction:

$$(E_0/2)[(1-\beta_c)/(1-\beta_c^2)^{\frac{1}{2}}],$$

where β_c is the velocity of the center of mass and is given by Eq. (A1). Therefore, the fraction of the total energy projected backward is

$$\rho=(1-\beta_c)/2. \qquad \text{(A4)}$$

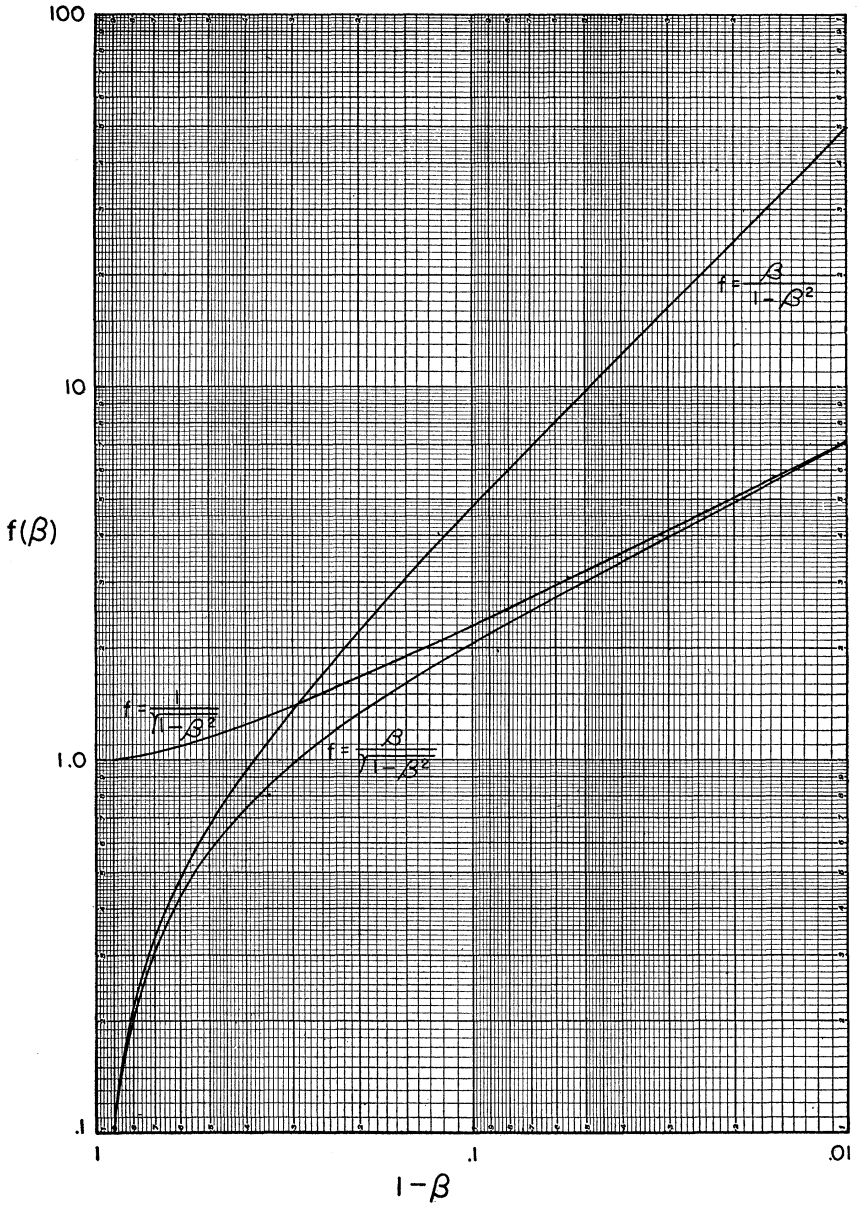

FIG. 25. The quantities $\beta/(1-\beta^2)$, $1/(1-\beta^2)^{\frac{1}{2}}$, $\beta/(1-\beta^2)^{\frac{1}{2}}$ plotted as functions of $1-\beta$.

In case (b) the light particles in the laboratory system come out at an angle ψ given by the equation (see Eq. (A3))

$$\tan\psi = (1-\beta_c^2)^{\frac{1}{2}}/\beta_c.$$

An easy calculation shows that if one assumes that the primary particles are incident upon the atmosphere with equal intensity from all directions above the horizon the fractional number of the secondary particles projected upwards has the following expression:

$$\rho = \frac{\tan\psi}{\pi}\int_0^1 \frac{\cos^{-1}y\,dy}{(1+y^2\tan^2\psi)^{\frac{3}{2}}}. \qquad \text{(A5)}$$

A graphical representation of the integral in Eq. (A5) as a function of ψ is given in Fig. 26. Table VIII shows the values of ρ computed, for several different values of p/Mc, according to both hypothesis (a) and hypothesis (b).

TABLE VII.

α	Nucleons E/Mc^2	Nucleons ψ	Mesons E/Mc^2	Mesons ψ
1	2.35	0°	3.17	25°
1.2	2.82	15°	2.70	25°
1.5	3.52	19.5°	2.00	25°
2.0	4.70	22°	0.82	24°
2.25	5.29	23°	0.23	0°

TABLE VIII. Fraction ρ of energy projected upwards in nuclear collisions.

p/Mc^2	Hyp. (a) ρ	Hyp. (b) ψ	Hyp. (b) ρ
2	0.19	52°	0.29
5	0.09	35°	0.19
10	0.046	25°	0.14
15	0.032	21°	0.11

The average momentum of the primary protons is probably of the order of 10 Bev. Table VIII shows that the corresponding value of ψ is between 5 and 14 percent. Actually, this estimate represents a lower limit because it is likely that a large fraction of the secondary light particles are produced by secondary nucleons of energy considerably smaller than 10 Bev. It is not possible to make a more precise estimate of the fraction of energy projected upwards until we know more of the details of the secondary processes in which the secondary particles arise. The above calculations, however, show that this fraction is not negligible.

30. Estimate of the Influence of the Angular Spread on the Total Energy of the Secondary Radiation Observed in the Vertical Direction

Let W_1 represent the energy (per second steradian) of *all* the secondary particles produced by primary rays incident vertically upon one square centimeter of the atmosphere. Let W_2 represent the energy (per second steradian) of the secondary particles projected vertically downward by *all* primary rays incident upon one square centimeter of the atmosphere. We want to calculate the ratio W_2/W_1. For this purpose, we assume that the primary rays are protons and that their interactions with atomic nuclei can be described as collisions between free nucleons. We assume further that, in the frame of reference in which the center of mass of the two colliding nucleons is at rest, the secondary particles produced in any one of these collisions have all the same energy E_0, and therefore the same momentum p_0. Since the results will turn out to be independent of E_0, this assumption does not imply any loss of generality. In the center of mass system, let $n_0(\psi_0)d\omega_0$ represent the average number of secondary particles projected within the element of solid angle $d\omega_0$ at an angle ψ_0 to the direction of the primary proton. Let $n(\psi)d\omega$, E, p represent the quantities corresponding to $n_0(\psi_0)d\omega_0$, E_0, p_0 in the laboratory system. If β_c represents the relative velocity of the two systems, the following equations hold:

$$p\cos\psi=(p_0\cos\psi_0+\beta_cE_0/c)/(1-\beta_c^2)^{\frac{1}{2}},$$
$$n(\psi)\sin\psi d\psi=n_0(\psi_0)\sin\psi_0 d\psi_0. \qquad \text{(A6)}$$

On the other hand, if we assume that the intensity of the primary radiation has a constant value $I^{(p)}$ in all directions above the horizon and is zero in all directions below the horizon, and if we indicate with $P_v d\omega$ the total momentum of the secondary particles projected within the element of solid angle $d\omega$ vertically downward by *all* primary rays incident upon one square centimeter of the atmosphere, we obtain for P_v

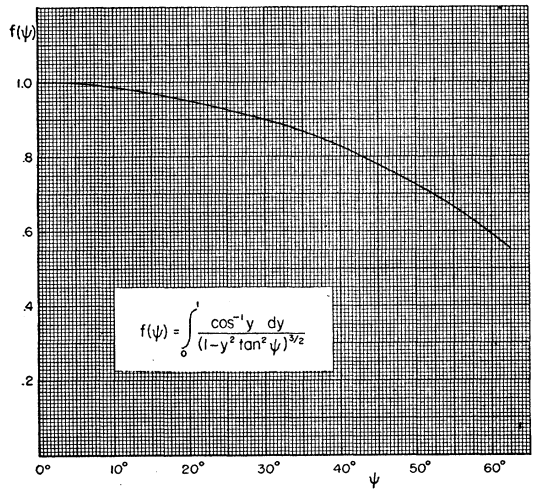

FIG. 26. Plot of the function $f(\psi)$. The quantity $\tan\psi f(\psi)/\pi$ represents the fractional number of secondary particles projected away from the earth, under the assumption that these particles are produced with an angular divergence ψ by a primary radiation distributed isotropically in the upper hemisphere.

the expression

$$P_v = 2\pi I^{(p)} \int_0^{\pi/2} pn(\psi) \cos\psi \sin\psi d\psi. \quad \text{(A7)}$$

If we make use of Eq. (A6), and consider that, for reasons of symmetry,

$$n_0(\psi_0) = n_0(\pi - \psi_0),$$

we can write Eq. (A7) as follows:

$$P_v = \frac{\beta_c E_0/c}{(1-\beta_c^2)^{\frac{1}{2}}} I^{(p)} N - \frac{2\pi I^{(p)}}{(1-\beta_c^2)^{\frac{1}{2}}} \times \int_{\psi_0'}^{\pi} n_0(\psi_0)[p_0 \cos\psi_0 + \beta_c E_0/c] \sin\psi_0 d\psi_0, \quad \text{(A8)}$$

where N is the total number of secondary particles produced in one collision and ψ_0' is the value of ψ_0 corresponding to $\psi = \pi/2$ and given by the equation

$$\cos\psi_0' = -\beta_c E_0/cp_0.$$

Since β_c is close to one, the angle ψ_0' is close to π and the contribution of the integral in Eq. (A8) is negligible except for the case in which, in the center of mass system, most of the secondary particles are produced in directions very close to the direction of the incident proton. If we assume that this is not the case and assume further that the secondary particles have relativistic velocities in the laboratory system, we obtain the following expression for the energy W_2 defined above:

$$W_2 = cP_v = [(\beta_c E_0)/(1-\beta_c^2)^{\frac{1}{2}}] N I^{(p)}. \quad \text{(A10)}$$

On the other hand, W_1 has the expression

$$W_1 = [(E_0)/(1-\beta_c^2)^{\frac{1}{2}}] N I^{(p)}. \quad \text{(A11)}$$

The ratio between W_2 and W_1 is therefore given by the equation

$$W_2/W_1 = \beta_c. \quad \text{(A12)}$$

For protons with momenta equal to 10 Bev/c, which corresponds to the average momenta of primary cosmic rays, the value of β_c is approximately 0.9, so that W_2 is 10 percent smaller than W_1. The actual difference between W_2 and W_1 may be even greater because some of the observed rays are probably produced by secondary nucleons of energy considerably lower than the energy of primary cosmic rays. It may be noted that in the limiting case that $n_0(\psi_0)$ is different from zero only for $\psi_0 = 0$ or $\psi_0 = \pi$, Eq. (A8) yields for W_2 the value

$$W_2 = [(E_0\beta_c + cp_0)/2(1-\beta_c^2)^{\frac{1}{2}}] N I^{(p)}$$

or, if the secondary particles have relativistic velocities in the center of mass system:

$$W_2 = [E_0/(1-\beta_c^2)^{\frac{1}{2}}][(\beta_c+1)/2] N I^{(p)}, \quad \text{(A10')}$$

from which it follows that

$$W_2/W_1 = (\beta_c+1)/2. \quad \text{(A12')}$$

For protons with momenta equal to 10 Bev/c the value of W_2/W_1 is, in this case, approximately 0.95.

BIBLIOGRAPHY

A1. H. M. Agnew, W. C. Bright, and D. Froman, Phys. Rev. **72**, 203 (1947).
A2. C. D. Anderson, R. V. Adams, P. E. Lloyd, and R. R. Rau, Phys. Rev. **72**, 724 (1947).
A3. C. D. Anderson, Rev. Mod. Phys. **20**, 334 (1948).
A4. P. Auger, R. Maze, and R. Chaminade, Comptes Rendus **213**, 381 (1941).

B1. G. Bernardini, B. N. Cacciapuoti, B. Ferretti, O. Piccioni, and G. C. Wick, Phys. Rev. **58**, 1017 (1940).
B2. G. Bernardini, Zeits. f. Physik **120**, 413 (1943).
B3. G. Bernardini, B. N. Cacciapuoti, and R. Querzoli, Phys. Rev. **73**, 335 (1948).
B4. H. A. Bethe, S. A. Korff, and G. Placzek, Phys. Rev. **57**, 573 (1940).
B5. H. A. Bethe, Phys. Rev. **70**, 821 (1946).
B6. P. M. S. Blackett, Proc. Roy. Soc. **A159**, 1 (1937).
B7. H. Bridge and B. Rossi, Phys. Rev. **71**, 379 (1947).
B8. H. Bridge, B. Rossi, and R. W. Williams, Phys. Rev. **72**, 257 (1947).
B9. H. Bridge, unpublished results.
B10. H. Bridge, W. E. Hazen, and B. Rossi, Phys. Rev. **73**, 179 (1948).
B11. R. B. Brode and M. A. Starr, Phys. Rev. **53**, 3 (1938).

C1. H. Carmichael and E. G. Dymond, Proc. Roy. Soc. **A171**, 321 (1939).
C2. J. Clay, C. G. T'Hooft, L. J. L. Dey, and J. T. Wiersma, Physica **4**, **2**, 121 (1937).
C3. J. H. Clay and P. H. Clay, Physica **2**, **10**, 1033 (1935).
C4. F. L. Code, Phys. Rev. **59**, 229 (1941).
C5. L. J. Cook, E. M. McMillan, J. M. Peterson and D. C. Sewell, Phys. Rev. **72**, 1264 (1947).
C6. M. Conversi and O. Piccioni, Nuovo Cimento **2**, 40 (1944).
C7. M. Conversi, E. Pancini, and O. Piccioni, Phys. Rev. **68**, 232 (1945).
C8. M. Conversi and O. Piccioni, Phys. Rev. **70**, 859 (1946).
C9. M. Conversi and O. Piccioni, Phys. Rev. **70**, 874 (1946).
C10. M. Conversi, E. Pancini, and O. Piccioni, Phys. Rev. **71**, 209 (1947).

D1. M. J. Daudin, Comptes Rendus **218**, 830 (1944).

E1. A. Ehmert, Zeits. f. Physik **106**, 751 (1937).
E2. P. Ehrenfest, Comptes Rendus **207**, 573 (1938).

F1. W. B. Fretter, Phys. Rev. **70**, 625 (1946).
F2. W. B. Fretter, Phys. Rev. **73**, 41 (1948).
F3. W. B. Fretter, private communication.
F4. E. Fünfer, Zeits. f. Physik **111**, 351 (1938).

G1. P. S. Gill, M. Schein, and V. Yngve, Phys. Rev. **72**, 733 (1947).
G2. S. E. Golian and E. H. Krause, Phys. Rev. **71**, 918 (1947).
G3. K. I. Greisen, Phys. Rev. **61**, 212 (1942).
G4. K. I. Greisen and N. G. Nereson, Phys. Rev. **62**, 316 (1942).
G5. K. I. Greisen, Phys. Rev. **63**, 323 (1943).

H1. E. Hayward, Phys. Rev. **72**, 937 (1947).
H2. W. E. Hazen, Phys. Rev. **63**, 213 (1943); **65**, 67 (1944).
H3. R. Hildebrand and B. J. Moyer, Phys. Rev. **72**, 1258 (1947).
H4. E. P. Hinck and B. Pontecorvo, Phys. Rev. **73**, 257 (1948).
H5. D. J. Hughes, Phys. Rev. **57**, 592 (1940).
H6. R. I. Hulsizer, Phys. Rev. **73**, 1252 (1948).

J1. L. Janossy, Proc. Roy. Soc. **A179**, 361 (1942).
J2. L. Janossy, C. B. McCusker, and G. D. Rochester, Phys. Rev. **64**, 345 (1943).
J3. L. Janossy and G. D. Rochester, Proc. Roy. Soc. **A183**, 181 (1944).
J4. L. Janossy and G. D. Rochester, Proc. Roy. Soc. **182**, 180 (1943).
J5. L. Janossy and G. D. Rochester, Proc. Roy. Soc. **A183**, 186 (1944).
J6. H. Jones, Rev. Mod. Phys. **11**, 235 (1939).
J7. T. H. Johnson, Rev. Mod. Phys. **11**, 207 (1939).

K1. H. P. Koenig, Phys. Rev. **69**, 590 (1946).
K2. H. L. Kraybill and P. J. Ovrebo, Phys. Rev. **72**, 351 (1947).

L1. C. M. G. Lattes, H. Muirhead, G. P. S. Occhialini, and C. F. Powell, Nature **159**, 694 (1947).
L2. C. M. G. Lattes, G. P. S. Occhialini, and C. F. Powell, Nature **160**, 463 (1947); **160**, 486 (1947).
L3. L. Leprince Ringuet, Comptes Rendus **221**, 406 (1945).

M1. R. Maze and R. Chaminade, Comptes Rendus **214**, 266 (1941).
M2. R. Maze and R. Chaminade, A. Freon, J. de phys. et rad. **7**, 202 (1945).
M3. R. S. Millikan, H. V. Neher, and W. H. Pickering, Phys. Rev. **63**, 234 (1943).
M4. P. A. Morris, W. F. G. Swann, and H. C. Taylor, Phys. Rev. **72**, 1263 (1947).

N1. N. Nereson and B. Rossi, Phys. Rev. **64**, 199 (1943).
N2. W. M. Nielsen, C. M. Ryerson, L. W. Nordheim, and K. Z. Morgan, Phys. Rev. **59**, 547 (1941).

O1. G. P. S. Occhialini and C. F. Powell, Nature **159**, 186 (1947).

P1. D. H. Perkins, Nature **159**, 126 (1947); **160**, 707 (1947).
P2. G. Pfotzer, Zeits. f. Physik **102**, 23 (1936).
P3. O. Piccioni, Phys. Rev. **73**, 411 (1948).
P4. W. M. Powell, Phys. Rev. **69**, 385 (1946).

R1. F. Rasetti, Phys. Rev. **59**, 613 (1941); **60**, 198 (1941).
R2. G. D. Rochester and M. Bound, Nature **146**, 745 (1940).
R3. G. D. Rochester, C. C. Butler, and S. K. Runcorn, Nature **159**, 227 (1947).
R4. B. Rossi, N. Hilberry, and J. D. Hoag, Phys. Rev. **57**, 461 (1940).
R5. B. Rossi and V. H. Regener, Phys. Rev. **58**, 837 (1940).
R6. B. Rossi and K. I. Greisen, Phys. Rev. **61**, 121 (1942).
R7. B. Rossi and S. J. Klapman, Phys. Rev. **61**, 414 (1942).
R8. B. Rossi and N. Nereson, Phys. Rev. **62**, 417 (1942).
R9. B. Rossi, M. Sands, and R. Sard, Phys. Rev. **72**, 120 (1947).
R10. B. Rossi and R. W. Williams, Phys. Rev. **72**, 172 (1947).

S1. U. Sala and G. Wataghin, Phys. Rev. **67**, 55 (1946); **70**, 430 (1946).
S2. M. Sands, Phys. Rev. **73**, 1338 (1948).
S3. M. Sands, unpublished results.
S4. R. Sard, and E. J. Althaus, Phys. Rev. **73**, 1251 (1948).
S5. M. Schein, W. P. Jesse, and E. O. Wollan, Phys. Rev. **59**, 615 (1941).
S6. M. Schein, Phys. Rev. **73**, 1239 (1948).
S7. R. P. Shutt, Phys. Rev. **61**, 6 (1942); **69**, 128 (1946); **69**, 261 (1946).
S8. T. Sigurgeirsson and A. Yamakawa, Phys. Rev. **71**, 319 (1947).
S9. M. S. Sinha, Phys. Rev. **68**, 153 (1945).
S10. J. H. Smith, Phys. Rev. **71**, 32 (1947).

T1. I. Tamm and S. Belenky, Phys. Rev. **70**, 660 (1946).
T2. H. E. Tatel and J. A. Van Allen, Phys. Rev. **73**, 87 (1948).
T3. H. K. Ticho, Phys. Rev. **71**, 463 (1947).
T4. H. K. Ticho and M. Schein, Phys. Rev. **73**, 81 (1948).
T5. H. K. Ticho, Phys. Rev. **73**, 1229 (1948).
T6. J. Tinlot, Phys. Rev., to be published.

V1. G. E. Valley, Phys. Rev. **72**, 772 (1947).
V2. G. E. Valley and B. Rossi, Phys. Rev. **73**, 177 (1948).
V3. G. E. Valley, unpublished results.
V4. J. A. Van Allen and H. E. Tatel, Phys. Rev. **73**, 245 (1948).

W1. J. A. Wheeler, Phys. Rev. **71**, 320 (1947).
W2. G. C. Wick, Nuovo Ciment, (June 1943).
W3. E. J. Williams and G. E. Roberts, Nature **145**, 102 (1940).
W4. J. G. Wilson, Proc. Roy. Soc. **A166**, 482 (1938).
W5. J. G. Wilson, Proc. Roy. Soc. **A172**, 517 (1939).
W6. J. G. Wilson, Proc. Roy. Soc. **A174**, 73 (1940).
W7. J. G. Wilson, Nature **158**, 415 (1946).
W8. V. C. Wilson, Phys. Rev. **53**, 337 (1938).

Y1. V. H. Yngve, M. Schein, and H. Kraybill, Phys. Rev. **73**, 1226 (1948).
Y2. L. C. L. Yuan and R. Ladenburg, private communication.